

# Vibrational spectroscopy of $\text{H}_2\text{He}^+$ and $\text{D}_2\text{He}^+$

Oskar Asvany<sup>a</sup>, Stephan Schlemmer<sup>a</sup>, Ad van der Avoird<sup>b</sup>, Tamás Szidarovszky<sup>c</sup>, Attila G. Császár<sup>c</sup>

<sup>a</sup>*I. Physikalisches Institut, Universität zu Köln, Zùlpicher Str. 77, 50937 Köln, Germany*

<sup>b</sup>*Theoretical Chemistry, Institute for Molecules and Materials, Radboud University, Nijmegen, The Netherlands*

<sup>c</sup>*Laboratory of Molecular Structure and Dynamics, Institute of Chemistry, ELTE Eötvös Loránd University and MTA-ELTE Complex Chemical Systems Research Group, H-1117 Budapest, Pázmány Péter sétány 1/A, Hungary*

---

## Abstract

Vibrational modes of the relatively strongly bound  $\text{H}_2\text{He}^+$  molecular ion and its deuterated congener  $\text{D}_2\text{He}^+$  are investigated by low-resolution multi-photon photodissociation spectroscopy, using a combination of a 4 K cryogenic ion-trap machine and the free-electron-laser FELIX. The band origins obtained are fully explained by accurate variational calculations of the rovibrational states of  $\text{H}_2\text{He}^+$  and  $\text{D}_2\text{He}^+$  based on the three-dimensional potential energy surface of Koner *et al.* [Phys. Chem. Chem. Phys. **21** (2019) 24976]. Results from second-order vibrational perturbation theory, based on a linear H–H–He equilibrium structure, agree well with those of the variational calculations for energies up to about  $1300\text{ cm}^{-1}$ . This suggests that  $\text{H}_2\text{He}^+$  and  $\text{D}_2\text{He}^+$  may either be considered as linear triatomic molecules with a degenerate bending mode, or as Van der Waals complexes with a strongly hindered rotation of He around the  $\text{H}_2^+$  and  $\text{D}_2^+$  subunits. The variational calculations show that in states close to the dissociation limit, [1794 and  \$1852\text{ cm}^{-1}\$  for \*para\*- and \*ortho\*- \$\text{H}\_2\text{He}^+\$ , respectively](#), the angular internal motion becomes delocalized. The low-resolution experiments corroborate the linear structure of the ions and identify the bright IR-active HH-stretch fundamental in  $\text{H}_2\text{He}^+$  at about  $1840\text{ cm}^{-1}$  and the DD-stretch fundamental in  $\text{D}_2\text{He}^+$  at about  $1309\text{ cm}^{-1}$ , both with an uncertainty of 0.5%, in good agreement with the calculations. The experiments also confirm the  $\text{H}_2^+$ –He bend and stretch fundamentals calculated at  $632$  and  $732\text{ cm}^{-1}$  and the  $\text{D}_2^+$ –He bend and stretch fundamentals at  $473$  and  $641\text{ cm}^{-1}$ , respectively.

*Keywords:* ion trap, free electron laser, vibrational spectroscopy,  $\text{H}_2\text{He}^+$ ,  $\text{D}_2\text{He}^+$

---

## 1. Introduction

$\text{H}_2\text{He}^+$  is a fundamental open-shell molecular system consisting of two protons, one  $\alpha$ -particle, and three electrons. To the best of our knowledge it was first detected, in 1925, in a mass spectrum by Hogness and Lunn [1]. This molecular ion, as well as larger complexes of the He-solvated series  $\text{H}_2\text{He}_n^+$ , have been unambiguously observed by mass-spectrometric means in a drift tube [2] and in He-droplet experiments [3].

As the  $\text{H}_2\text{He}^+$  molecular ion is composed of the only elements abundantly available at the very beginning of the universe, it might have been formed at the earliest stages of chemical evolution. Most importantly, it must have played a crucial role as the intermediate in the fundamental inelastic or reactive collisions between  $\text{H}_2^+$  ions and He atoms, as well as in the collision between the first molecule of the primordial universe, the  $\text{HeH}^+$  ion, detected recently [4] in the hot gas of the planetary nebula NGC 7027, and hydrogen atoms. Therefore, the detailed knowledge of at least the  $\tilde{X}^2\Sigma^+$  potential energy surface (PES) of  $\text{H}_2\text{He}^+$  [5, 6] is of fundamental importance for astronomy (the excited electronic states of  $\text{H}_2\text{He}^+$  are well separated from the ground state). Due to the presence of two H atoms, the molecular ion has two nuclear-spin isomers, *ortho*- and *para*- $\text{H}_2\text{He}^+$  (a similar statement holds for  $\text{D}_2\text{He}^+$ ).

The  $\tilde{X}^2\Sigma^+$  PES of  $\text{H}_2\text{He}^+$  has been explored experimentally by numerous reactive scattering experiments through the reaction  $\text{H}_2^+(v) + \text{He}$  and its isotopic variants [7, 8, 9, 10, 11], where  $v$  is the vibrational quantum number. Due to its endothermicity of  $0.806\text{ eV}$  [7], the reaction exhibits strong enhancement upon vibrational excitation.

Experimental investigations of the (ro)vibrational bound states of  $\text{H}_2\text{He}^+$  *via* spectroscopy are extremely sparse. The only investigation available up to date, due to Carrington and co-workers [12, 13], is an unusual one, in which a mass-selected and highly-excited beam of  $\text{H}_2\text{He}^+$  ions was subjected to microwave radiation. Those ions very close to the dissociation limit were subsequently dissociated by an electric field and the  $\text{H}_2^+$  fragments counted as a function of the excitation frequency. Several microwave and millimeter-wave transitions have been observed for  $\text{H}_2\text{He}^+$  [13]; in particular, a *para* transition close to  $21.8\text{ GHz}$  and an *ortho* transition at  $15.2\text{ GHz}$ , exhibiting fine- and hyperfine substructure. As the states involved in these transitions are close to the dissociation limit, the interpretation of these spectra provided a considerable challenge for first-principles computations [6].

Scattering and photodissociation simulations on the related PESs, as well as bound rovibrational states and transitions between these states in the ground electronic state of  $\text{H}_2\text{He}^+$  have all been calculated with increasing accuracy during the last decades [6, 12, 14, 15, 16, 17, 18, 19, 20, 21, 22, 23, 24, 25].

---

*Email address:* [asvany@ph1.uni-koeln.de](mailto:asvany@ph1.uni-koeln.de) (Oskar Asvany)

In the most recent work [6], high-level *ab initio* computations were used to construct two very similar analytical PESs, accurately including the important long-range part of the interaction between  $\text{H}_2^+$  and He. Both PESs feature a global minimum with an equilibrium dissociation energy of  $D_e = 2735 \text{ cm}^{-1}$  at the linear H–H–He configuration. One of these PESs, called FCI, is heavily utilized during the present study. In Ref. [6], computations of the bound states on these PESs were executed with two different variational techniques, one utilizing the DVR3D code [26] and the other a coupled-channels variational method (CCVM) [27]. Both yielded the lowest bound state at  $-1794 \text{ cm}^{-1}$ , which corresponds to a dissociation energy of  $D_0 = 1794 \text{ cm}^{-1}$  for *para*- $\text{H}_2\text{He}^+$  and  $D_0 = 1852 \text{ cm}^{-1}$  for *ortho*- $\text{H}_2\text{He}^+$  (the latter is higher by about  $58 \text{ cm}^{-1}$  due to dissociation into  $\text{H}_2^+(j = 1)$ , see also Table 1, where  $j$  is the quantum number associated with the rotation of the diatomic  $\text{H}_2^+$  unit). The PES of  $\text{H}_2\text{He}^+(\tilde{X}^2\Sigma^+)$  is thus characterized by a relatively deep well and allows the ion to harbour more than a dozen vibrational states and hundreds of bound rovibrational states with total angular momenta up to  $J = 21$ , where  $J$  is the quantum number corresponding to the overall rotation of the molecular ion. In another study, a plethora of rovibrational resonances [28] with widely different lifetimes were found beyond the dissociation limit, though utilizing a different, less sophisticated PES [29]. All the bound states essentially correspond to strongly coupled  $\text{H}_2^+$ –He stretching and bending motions, while the H–H stretch motion is expected to be around  $1800 \text{ cm}^{-1}$ , which is just below the dissociation limit of *ortho*- $\text{H}_2\text{He}^+$ . The high quality of the recent first-principles computations facilitate reliable assignment suggestions [6], in particular for the near-dissociation spectra measured some 20 years ago [13]. Since the dissociation energy is in the infrared range probed by our experiments, one must address the question whether the spectral features observed can be interpreted as those belonging to a semirigid linear molecule or require sophisticated variational treatments whereby rigidity of the molecular ion is not assumed.

To the best of our knowledge, no experimental (ro)vibrational spectroscopic data, apart from those already mentioned [12, 13], are available for this molecule and its isotopologues, despite the potential astronomical relevance these data possess. To improve our knowledge about the structure and dynamics of the  $\text{H}_2\text{He}^+$  and  $\text{D}_2\text{He}^+$  systems, we need to obtain high-resolution rovibrational and rotational spectra of these elusive molecules, preferentially yielding their fundamental transitions and beyond. On our path to generate this knowledge, we present here the first low-resolution vibrational fingerprints of  $\text{H}_2\text{He}^+$  and  $\text{D}_2\text{He}^+$ , obtained by using a combination of a 4 K cryogenic ion trap apparatus [30] and the widely tunable free electron laser at the FELIX facility [31]. Furthermore, we present accurate variational calculations of the rovibrational states and transitions of  $\text{H}_2\text{He}^+$  and  $\text{D}_2\text{He}^+$ , based on the three-dimensional FCI potential surface described in Ref. [6], as well as second-order vibrational perturbation theory (VPT2) [32, 33, 34] calculations based on the linear H–H–He equilibrium structure.

As to the structure of the rest of this paper, the experimental

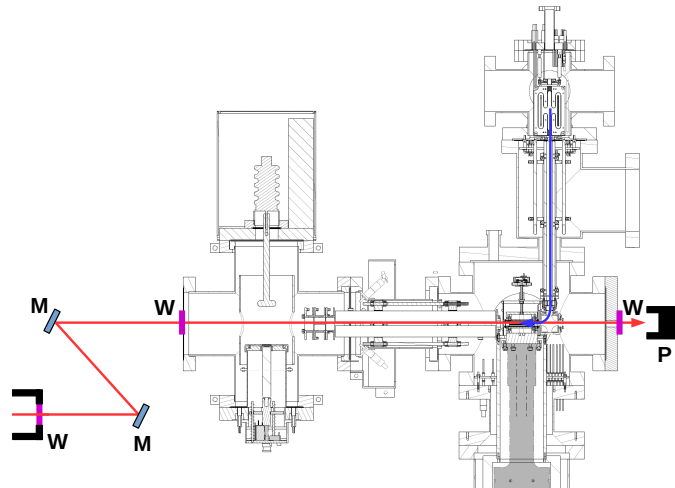


Figure 1: Scheme showing the path of the FELIX laser beam (red) through the 22-pole trapping machine FELION. After exiting the evacuated FELIX beam-line through a window (W, on the very left), the pulsed laser beam enters a purged laser table containing two guiding mirrors (M), which steer the beam through the 22-pole trapping machine into a power meter (P). All windows (W) are made of KRS-5, which permits experiments down to about  $250 \text{ cm}^{-1}$ . The blue arrow indicates the way of the ion bunches from the storage ion source into the 22-pole ion trap.

details are given in Section 2, while the rovibrational eigenstate calculations are described in Section 3. Sections 4 and 5 summarize the spectral results obtained during this study for  $\text{H}_2\text{He}^+$  and  $\text{D}_2\text{He}^+$ , respectively, as well as a comparison of the experimental results with their computational counterparts, aiding the understanding of all the experimental features. Finally, in Section 6, we sketch a path how to obtain high-resolution spectra for the two ions investigated. The approach outlined is similar to that taken recently for the proton-helium cations  $\text{HHe}_n^+$  [35, 36, 37]. Section 6 also contains a summary of the results of this study.

## 2. Experimental Details

### 2.1. Experimental setup

The experimental setup employed during this study is elucidated using the scheme shown in Fig. 1. The central part of this experiment is a 22-pole ion trapping machine, called FELION [30], which is nearly identical to the one described in detail in Ref. [38]. Molecular ions are produced in an external storage ion source. In this source, electrons with small kinetic energy ( $< 20 \text{ eV}$ ) are used to ionize (and also fragment) the precursor gas. After mass selection in a linear quadrupole mass filter, an ensemble of several ten thousand ions is injected into the cold 22-pole ion trap [39] and stored there for typically a few seconds. For a standard experiment, the trap is held at its lowest temperature,  $T = 4 \text{ K}$ . A  $\sim 100 \text{ ms}$ -long He pulse at the beginning of the trapping cycle cools the ions and leads to the efficient formation of cation-helium complexes by ternary collisions. During the trapping time, the ionic complexes are exposed to the tunable IR pulses of FELIX [31] (see Fig. 1). After the storage period, the ion cloud is extracted from the trap,

mass-selected by a second mass filter, and the number of ions in a pre-selected mass channel is counted by an effective ion counter. Such storage cycles are repeated typically 2-3 times to improve the signal-to-noise ratio, after which the FELIX laser is tuned to the next frequency setting.

The FELIX laser is operated at its maximum repetition rate of 10 Hz. The pulses have an energy content varying from 8 to 14 mJ (at the user station), depending on the wavelength region. The beam enters and exits the 22-pole trapping machine by a pair of KRS-5 windows, after which it is stopped by a power meter (see Fig. 1). The laser power is constantly monitored by this meter in order to normalize the obtained spectra to power. The bandwidth of FELIX is transform-limited with a typical resolution of 0.5% full width at half maximum of the central frequency (*e.g.*,  $\Delta\nu = 5 \text{ cm}^{-1}$  at  $\nu = 1000 \text{ cm}^{-1}$ ). With this resolution, we are generally not able to resolve single rovibrational lines, but can only recover the envelopes of the vibrational bands. In our experiments, the trapping cycle time of 3 s was synchronized to the frequency of the main electrical power supply. By this, synchronization with the 1 s cycle of the cold head was achieved (important for stable tagging with He at 4 K), as well as synchronization to the 10 Hz laser pulses of FELIX.

## 2.2. Experimental conditions

In the current experiment, we used hydrogen gas (Linde 6.0) in the ion source to produce  $\text{H}_2^+$ . In order to avoid excitation of the produced ions, the electron energy was reduced to about 17 eV and the hydrogen gas was diluted in helium in a ratio 1:4 ( $\text{H}_2:\text{He}$ ), so that efficient quenching/removal of excited  $\text{H}_2^+$  could occur. Furthermore, the gas pressure in the source was minimized in order to keep the leakage of  $\text{H}_2$  gas into the ion trap region to a minimum. The first quadrupole mass filter was driven at a high frequency of 2.74 MHz in order to efficiently transmit and select the ions with mass 2 u. When  $\text{H}_2^+$  is injected into the 4 K cold ion trap filled with helium (and a small contamination of  $\text{H}_2$ ), a series of processes occur, which are illustrated and explained in Fig. 2, showing a typical mass spectrum observed. Similarly, for the investigation of  $\text{D}_2\text{He}^+$ , a 4:1 mixture of helium and deuterium (Praxair 2.8) is admitted to the source, and the first mass filter is set to select  $\text{D}_2^+$  ions at mass 4 u. A typical mass spectrum recorded after a trapping time of 1.5 s is shown in Fig. 3, exemplifying the efficient production of  $\text{D}_2\text{He}^+$ , as well as  $\text{D}_2\text{He}_2^+$ .

The  $\text{H}_2\text{He}^+$  and  $\text{D}_2\text{He}^+$  ions are formed in the trap in the first 100 ms of the He pulse and the rest of the trapping time they are irradiated by the FELIX beam. When the FELIX frequency is on resonance, IR photodissociation (IRPD) occurs, *e.g.*,



which is observed as a decrease in the number of the detected parent ion  $\text{H}_2\text{He}^+$  (similar for  $\text{D}_2\text{He}^+$ ). In the dissociation process one photon ( $n = 1$ ) or more photons ( $n > 1$ ) may be needed to reach the dissociation limit. These photons might be absorbed sequentially if the time in-between these events is

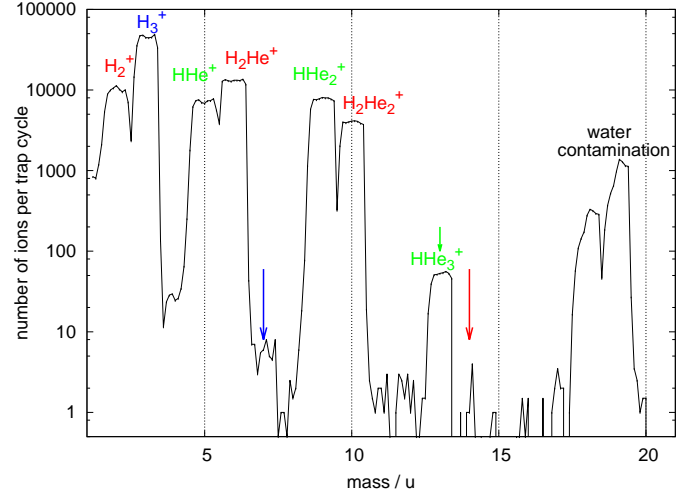


Figure 2: A typical mass spectrum illustrating the rich chemistry when  $\text{H}_2^+$  ions are injected into a 4 K cloud of He atoms. The mass-selected  $\text{H}_2^+$  ions have been injected into the 22-pole trap and stopped by a  $\sim 100$  ms-long He pulse. The resulting ion cloud has been extracted from the trap after a trapping time of 1.5 s. Small  $\text{H}_2$  contaminations in the trap (contained in the He pulse and primarily leaking in from the ion source) lead to the efficient formation of  $\text{H}_3^+$  (mass 3 u) by the reaction  $\text{H}_2^+ + \text{H}_2 \rightarrow \text{H}_3^+ + \text{H}$ . Additionally, excited hydrogen ions initiate the reaction  $\text{H}_2^{*+} + \text{He} \rightarrow \text{HHe}^+ + \text{H}$  [8, 10]. Further ternary collisions with He atoms lead from  $\text{HHe}^+$  (mass 5 u) to  $\text{HHe}_2^+$  (mass 9 u), and even  $\text{HHe}_3^+$  can be detected (mass 13 u, green arrow). Of interest in this work is the ternary reaction  $\text{H}_2^+ + 2\text{He} \rightarrow \text{H}_2\text{He}^+ + \text{He}$ , leading to the formation of  $\text{H}_2\text{He}^+$  (mass 6 u). A second He atom can also be attached, leading to  $\text{H}_2\text{He}_2^+$ , but not a third (see red arrow), being an indication that  $\text{H}_2\text{He}_2^+$  has a linear symmetric configuration, in accordance with our *ab initio* computations (not detailed). The ion signal at mass 18 and 19 u is due to water contamination contained in the He pulse.

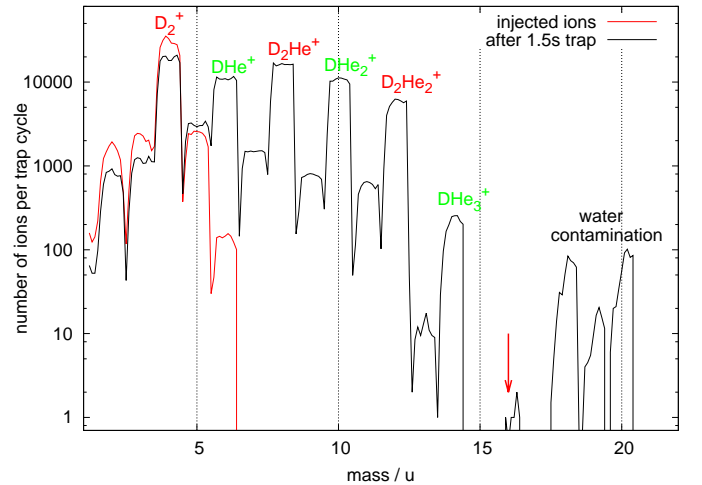


Figure 3: Same as Fig. 2 but with  $\text{D}_2^+$  injected into the 4 K cold trap filled with an intense He pulse at the beginning of the trapping sequence. Shown is the mass-selected injected ion ensemble and the ion ensemble after 1.5 s trapping time, during which reactions with He and small contaminations of  $\text{H}_2$  and  $\text{D}_2$  occur. Again, up to two He atoms can attach to  $\text{D}_2^+$  under the current experimental conditions ( $\text{D}_2\text{He}_3^+$  counts are negligible, see red arrow).

shorter than the radiative lifetime of the excited state. The corresponding excitation process is called multiple photon absorption. Alternatively, because of the very short light pulses of the FELIX laser the excitation process can also occur in a coherent fashion called multi-photon absorption. The actual mechanism

will depend on several factors and lead to different band-profiles as will be discussed below.

The spectral signal for the measurements is obtained by counting the number of parent ions,  $c(f)$ , as function of the FELIX frequency  $f$  (in  $\text{cm}^{-1}$ ). This is converted into a normalized spectrum by using  $s(f) = (c_0 - c(f))/(c_0 \cdot P(f))$ , with  $P(f)$  being the frequency-dependent laser power and  $c_0$  the  $\text{H}_2\text{He}^+$  (or similarly  $\text{D}_2\text{He}^+$ ) counts with the FELIX radiation being off-resonant.

### 3. Theory

#### 3.1. Preliminaries

In its  $\tilde{X}^2\Sigma^+$  ground electronic state  $\text{H}_2\text{He}^+$  may be considered as a semi-rigid open-shell molecular ion with a linear equilibrium structure of  $C_{\infty v}$  point-group symmetry. Nevertheless, especially in its higher rovibrational states, we may also consider  $\text{H}_2\text{He}^+$  as a more or less floppy Van der Waals complex that tunnels between two equivalent linear equilibrium structures with He on either side of the  $\text{H}_2^+$  subunit and assign it to the permutation-inversion symmetry group  $G_4$ , also called molecular-symmetry (MS) group  $C_{2v}(\text{M})$  [40]. As mentioned above, this molecular ion has two nuclear-spin isomers, *ortho* and *para* (*o/p*). The fine and hyperfine splittings in the rovibrational spectrum of  $\text{H}_2\text{He}^+$ , [due to coupling of electron spin and total nuclear spin, and coupling of the resultant to the rotational angular momentum of the nuclei](#), are predicted to be quite small, on the order of  $0.003 \text{ cm}^{-1}$  [6, 12, 18]. Therefore, they can be safely neglected during the rovibrational calculations and the simulation of the low-resolution results studied here. When considering  $\text{H}_2\text{He}^+$  and  $\text{D}_2\text{He}^+$  as semi-rigid molecules, their vibrational modes can be approximately described by the  $(\nu_1 \nu_2 \nu_3) \equiv (\nu_r \nu_b \nu_s)$  notation [14, 15], with  $\nu_i$  labeling the quanta for the H–H stretch, H–H–He bend, and H–He stretch, respectively. At higher vibrational excitation this notation is not particularly meaningful due to the strong mixing of the modes. The bend mode labeled with  $\nu_2$  has vibrational angular momentum  $l_{\nu_2}$  ranging from  $-\nu_2$  to  $+\nu_2$  in steps of 2. Furthermore,  $J$  is the quantum number corresponding to the overall rotation of the molecular ion. The quantum number  $k$ , the projection of  $\mathbf{J}$  and of  $\mathbf{j}_{\text{H}_2^+}$  or  $\mathbf{j}_{\text{D}_2^+}$  onto the axis  $\mathbf{R}$  that points from the  $\text{H}_2^+(\text{D}_2^+)$  center of mass to the He nucleus (see Fig. 4), is the same as  $l_{\nu_2}$  in the semi-rigid molecule notation. Usually one labels states with the absolute value of  $k$  and distinguishes the parity-adapted plus and minus combinations of  $+k$  and  $-k$  functions by their spectroscopic parity  $e$  and  $f$  [41].

#### 3.2. Structure and energetics

The open-shell  $\text{H}_2\text{He}^+$  and  $\text{D}_2\text{He}^+$  molecular ions contain only three electrons; thus, their electronic structure can be investigated at the full configuration interaction (FCI) level, which is equivalent to coupled cluster theory with all single, double, and triple substitutions (CCSDT) [42]. Although an accurate PES at the FCI level was already calculated by Koner *et al.* [6] and we used this potential in our variational calculations, we performed additional electronic-structure calculations

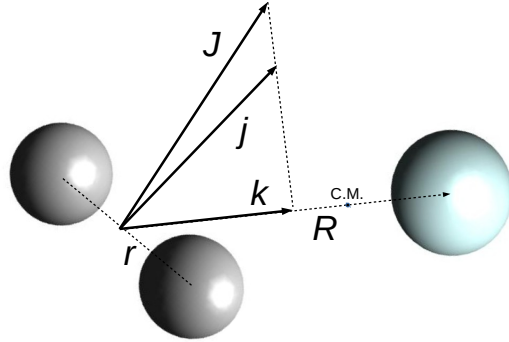


Figure 4: Sketch of the angular momentum vectors in the  $\text{H}_2\text{He}^+$  system.  $\mathbf{J}$  and  $\mathbf{j}_{\text{H}_2^+}$  have the same projection  $k$  onto the  $\mathbf{R}$  axis. The origin of  $\mathbf{J}$  has been shifted from the center-of-mass of the overall complex (C.M.) to the center-of-mass of  $\text{H}_2^+$  for easier viewing.

in view of our VPT2 study of the rovibrational levels and in order to compute the dipole moment surface that we used in our calculations of the transition line strengths. We utilized the CFOUR [43], the MRCC [42, 44, 45], and the Gaussian16 [46] codes and employed the aug-cc-pVTZ and aug-cc-pVQZ basis sets, members of the correlation-consistent (cc) family [47] of atom-centered, fixed-exponent, Gaussian basis functions.

According to the aug-cc-pVQZ FCI (CCSDT) optimization, the equilibrium HH and HHe distances in the global minimum of  $\tilde{X}^2\Sigma^+$   $\text{H}_2\text{He}^+$  are  $r_e(\text{HH}) = 1.098 \text{ \AA}$  and  $r_e(\text{HHe}) = 1.024 \text{ \AA}$ , respectively. The transition state (TS) connecting the two equivalent minima of  $\text{H}_2\text{He}^+$  (He on the left and right of the central  $\text{H}_2^+$  unit) is characterized by  $r_e(\text{HH}) = 1.049 \text{ \AA}$  and  $r_e(\text{HHe}) = 2.159 \text{ \AA}$  (no primary bond between H and He) and it has  $C_{2v}$  point-group symmetry. The energy difference between the global minimum and the TS, without vibrational correction, is  $2383 \text{ cm}^{-1}$ ; thus, somewhat less than  $D_e$ . In line with the structural characteristics of the TS, its harmonic wavenumbers are  $2361(a_1)$ ,  $227(a_1)$ , and  $278i(b_2) \text{ cm}^{-1}$ . All these values were obtained at the aug-cc-pVQZ FCI level. Thus, at the highest energies of IR excitation the dynamics switches from a single-minimum to a symmetric double-well problem, with appropriate consequences for the measurable spectra of the molecular ion.

#### 3.3. VPT2 results

For  $\text{H}_2\text{He}^+$ , the harmonic fundamentals at the aug-cc-pVQZ FCI[UCCSD(T)] level are  $1937[1940]$ ,  $721[730]$ , and  $988[992] \text{ cm}^{-1}$ , showing the consistency of the results. The VPT2 anharmonic corrections [34] computed are only substantial for  $\nu_3$ , at the aug-cc-pVQZ FCI[UCCSD(T)] level they are  $-103(-100)$ ,  $-73(-79)$ , and  $-242(-247) \text{ cm}^{-1}$ , respectively (quite good agreement even for the anharmonic corrections). Thus, the *ab initio* VPT2 computations predict an intense  $\nu_1(\sigma^+)$  fundamental at  $1835 \text{ cm}^{-1}$ . [Furthermore, the same VPT2 computations predict the first overtone of the bend,  \$2\nu\_2\$ , at  \$1258 \text{ cm}^{-1}\$ , and the overtone of the HHe stretch,  \$2\nu\_3\$ , at  \$1280 \text{ cm}^{-1}\$ .](#)

At the aug-cc-pVQZ FCI[UCCSD(T)] levels the harmonic fundamentals of  $\text{D}_2\text{He}^+$  are  $1371[1370]$ ,  $523[523]$ , and

807[806]  $\text{cm}^{-1}$ , adding confidence to the reliability of the computed results. The VPT2 results of this study, corresponding to the aug-cc-pVQZ FCI level of electronic-structure theory, are as follows. The anharmonic DD stretch fundamental,  $\nu_1$ , is at 1299  $\text{cm}^{-1}$  and it has high intensity. The doubly-degenerate bending fundamental,  $\nu_2$ , is at 481  $\text{cm}^{-1}$ , while the DHe stretch fundamental,  $\nu_3$ , is at 644  $\text{cm}^{-1}$ . The VPT2 computations predict the first overtone of the bend at 943  $\text{cm}^{-1}$ , with a surprisingly large intensity, larger than that of the DHe stretch fundamental. The overtone of the DHe stretch,  $2\nu_3$ , is at 1175  $\text{cm}^{-1}$ , with an intensity similar to that of the other overtone. There are no predicted bands of any intensity between 1300 and 1800  $\text{cm}^{-1}$ . The first band with significant intensity is the stretch combination band,  $\nu_1 + \nu_3$ , at 1975  $\text{cm}^{-1}$ .

The vibrational anharmonicities mentioned above, obtained through the VPT2 scheme [34], have been computed with the help of the CFOUR [43] package. The VPT2 treatment takes into account neither that the lowest dissociation energy ( $D_0$ ) of  $\text{H}_2\text{He}^+$  is less than  $\nu_1$  nor the double-well nature of the PES of  $\text{H}_2\text{He}^+$ . When the VPT2 results are meaningful, that is at lower-energy excitations, they fully support the variational results of this study (*vide infra*). Thus, in what follows only the variational results will be discussed in detail; the VPT2 results are listed, alongside the variational ones, in Table 3 (*vide infra*).

### 3.4. Dynamics

Two different, independently coded, variational nuclear-motion approaches were employed to calculate the rovibrational energy levels and wavefunctions of  $\text{H}_2\text{He}^+$  and  $\text{D}_2\text{He}^+$ . In the first one the  $T_{l\leftarrow k}$  one-photon dipole transition amplitudes in the spectrum of  $\text{H}_2\text{He}^+$  and  $\text{D}_2\text{He}^+$  were evaluated as  $T_{l\leftarrow k} \propto \langle \Psi_l | \hat{\mu} e^{(p)} | \Psi_k \rangle \delta(E_l - E_k \pm \hbar\omega_p)$ , where  $e^{(p)}$  and  $\hbar\omega_p$  are the polarization vector and the photon energy of the probe pulse, respectively, and  $\hat{\mu}$  is the dipole vector. The rovibrational  $|\Psi_i\rangle$  wave functions and the  $E_i$  eigenenergies were obtained by solving the time-independent rovibrational Schrödinger equation in full dimension, employing the variational D<sup>2</sup>FOPI protocol [48] and the PES of Koner *et al.* [6]. In the D<sup>2</sup>FOPI program, the rovibrational Hamiltonian of a triatomic molecule is constructed in an orthogonal coordinate system (Jacobi coordinates in this study) using a mixed discrete variable representation (DVR) and finite basis representation [49] along the vibrational degrees of freedom, and symmetry adapted Wigner matrices as rotational basis functions. The  $C_{2v}(\text{M})$  molecular symmetry is utilized as described in Ref. [50], and the eigenpairs are obtained by a variant of the Lánczos iterative eigensolver. For each value of  $J$  and each irreducible representation of the  $C_{2v}(\text{M})$  molecular symmetry group, we employed in the calculations a complete set of rotational basis functions, 35 potential-optimized (PO) spherical DVR basis functions [48] along the  $r$  coordinate (H-H stretch), 75 PO spherical DVR basis functions along the  $R$  coordinate ( $\text{H}_2$ -He stretch), and 30 associated Legendre functions along the Jacobian angle coordinate  $\theta$ . The coordinate ranges  $R \in (0, 15) a_0$  and  $r \in (0, 4) a_0$ , and the atomic masses  $m_{\text{H}} = 1.007\,825\,032\,1 u$ ,  $m_{\text{D}} = 2.014\,101\,778 u$ , and  $m_{\text{He}} = 4.002\,603\,249\,7 u$  were employed. Because the FELIX

pulse was linearly polarized during the experiments, the framework detailed in Ref. [23] could be followed for the theoretical evaluation of the dipole matrix elements.

The second variational approach employed is the coupled-channels variational method (CCVM) [27]. This method was already used in Ref. [6] to compute the bound rovibrational states of  $\text{H}_2\text{He}^+$ , here it is also used to compute the bound states of  $\text{D}_2\text{He}^+$ . It is similar to a coupled-channels scattering calculation, but instead of propagating the radial coordinate  $R$  to solve the CC differential equations it uses a basis also in  $R$  and obtains the desired number of eigenstates of the Hamiltonian matrix with the iterative Davidson algorithm [51]. The angular channel basis expressed in body-fixed (BF) coordinates is described for the most general case in Eq. (16) of Ref. [52], here it just contains symmetry-adapted products of spherical harmonics for the internal rotation of  $\text{H}_2^+$  in the  $\text{H}_2\text{He}^+$  ion and symmetric rotor functions for the overall rotation of the ion. The spherical harmonic basis was limited to  $j_{\text{H}_2^+}$  from 0 to 19, with even values of  $j_{\text{H}_2^+}$  for *para*- $\text{H}_2^+$  and odd values for *ortho*- $\text{H}_2^+$ . The  $r$  basis contained the  $v = 0 - 7$  eigenfunctions of the free  $\text{H}_2^+$  Hamiltonian for  $j_{\text{H}_2^+} = 0$  on a grid of 110 equidistant points with  $r = 0.25 - 5.5 a_0$ . The basis in  $R$ , the He- $\text{H}_2^+$  center-of-mass distance, was obtained as described in Ref. [6] on an equidistant 357-point grid with  $R = 2 - 50 a_0$ . In order to converge also near-dissociative states, we included 120 radial basis functions in the 3D direct-product basis. We used somewhat finer grids in our CCVM calculations for  $\text{D}_2\text{He}^+$ , but the same basis except in the  $\text{D}_2^+$  vibrational coordinate  $r$  where the basis was limited to  $v = 0 - 5$ , because we established that this is amply sufficient for convergence. Even values of  $j_{\text{D}_2^+}$  correspond to *ortho*- $\text{D}_2^+$  and odd values to *para*- $\text{D}_2^+$ . In the calculations of the vibrational bases in the coordinates  $r$  and  $R$ , as well as in the full 3D calculations we replaced the hydrogen atomic mass by that of deuterium.

The dipole moment surfaces (DMS) of  $\text{H}_2\text{He}^+$  and  $\text{D}_2\text{He}^+$  were obtained from the *ab initio* values calculated on a uniform grid in the Jacobi coordinates  $r$ ,  $R$ , and  $\theta$ , consisting of 11 900 points. The  $z$ - and  $x$ -components of the dipole vector  $\mu$  in the BF frame were replaced by spherical components:  $\mu_0 = \mu_z$  and  $\mu_{\pm 1} = \mp \mu_x / \sqrt{2}$ . Then, they were fitted with the appropriate angular expansion functions given in general in Eq. (36) of Ref. [52], which in this case are simply Racah-normalized spherical harmonics  $C_{L,M}(\theta, 0)$  with  $M$  values 0,  $\pm 1$  equal to the corresponding spherical dipole components and  $L$  ranging from 0 to 14 in steps of 2. The *ab initio* dipole values were calculated for  $R = (1, 10) a_0$  and  $r = (0.5, 4) a_0$ . Since at  $R = 10 a_0$  they are already very close to the isotropic long-range dipole moment that originates from a charge of  $+e$  at the center of  $\text{H}_2^+$  and the charge-induced dipole on the He atom, they could be extended to the largest  $R$  value of  $50 a_0$  in our grid with the use of the corresponding long-range formula. The extension to the full  $r$  grid is not important, since all of the calculated 3D wave functions have completely decayed for  $r < 0.5 a_0$  and  $r > 4 a_0$ . After these extensions of the dipole function, we obtained its values on our  $R$  and  $r$  grids by cubic-spline interpolations and calculated its matrix elements over the vibrational bases in  $R$  and  $r$ . A general formula for the angular matrix elements of the

Table 1: Rovibrational energy levels of  $\text{H}_2\text{He}^+$  from CCVM calculations. The approximate quantum number  $k$  corresponds to the projection of  $J$  onto the  $\text{H}_2^+$ -He axis  $R$ ; different values of  $k$  are mixed by Coriolis coupling.

| <i>para</i> - $\text{H}_2\text{He}^+$ , dissociation limit 0: $\text{H}_2^+(v = 0, j = 0) + \text{He}$                          |            |            |            |            |            |            |            |
|---|------------|------------|------------|------------|------------|------------|------------|
| parity $e$  |            |            |            |            |            |            |            |
| $k$   | $J = 0$    | $J = 1$    | $J = 2$    | $J = 3$    | $J = 4$    | $J = 5$    | $J = 6$    |
| 0   | -1793.9100 | -1785.7456 | -1769.4259 | -1744.9687 | -1712.4011 | -1671.7591 | -1623.0883 |
| 1   |            | -1153.8922 | -1138.1614 | -1114.6113 | -1083.2991 | -1044.3048 | -997.7342  |
| 0   | -1062.3122 | -1054.9462 | -1040.2212 | -1018.1510 | -988.7549  | -952.0563  | -908.0805  |
| 0   | -659.8318  | -652.0388  | -636.4863  | -613.2428  | -582.4166  | -544.1638  | -498.7059  |
| 1   |            | -562.4269  | -554.2751  | -538.3626  | -515.9214  | -487.2021  | -452.3557  |
| 2   |            |            | -539.8618  | -515.3600  | -484.3458  | -447.0176  | -403.6516  |
| 0   | -538.2728  | -531.0274  | -516.5188  | -494.6779  | -465.3325  | -428.2043  | -383.0657  |
| 0   | -300.6222  | -295.0990  | -284.0509  | -267.5138  | -245.6279  | -218.7084  | -187.2875  |
| 1   |            | -212.5983  | -201.4328  | -187.4625  | -168.8983  | -144.8920  | -115.0667  |
| 0   | -214.0134  | -209.6966  | -200.8680  | -184.7947  | -163.2747  | -137.2054  | -106.9923  |
| 2   |            |            | -177.3430  | -160.3962  | -137.6056  | -108.8875  | -74.2254   |
| 1   |            | -154.6440  | -139.8068  | -118.1424  | -90.1826   | -57.0053   | -32.0779   |
| 0   | -109.8312  | -105.4874  | -96.9863   | -84.7071   | -69.1914   | -50.6674   | -17.3708   |
| 0   | -60.7977   | -57.1436   | -49.8068   | -38.7917   | -24.3893   | -8.0949    |            |
| 0   | -16.0065   | -14.3159   | -11.0230   | -6.3126    | -0.6845    |            |            |
| 0   | -1.5401    | -0.9845    | -0.0804    |            |            |            |            |
| parity $f$  |            |            |            |            |            |            |            |
| 1   |            | -1153.5711 | -1137.1921 | -1112.6540 | -1079.9935 | -1039.2603 | -990.5168  |
| 1   |            | -561.1550  | -551.7892  | -533.5403  | -507.9355  | -475.2482  | -435.6702  |
| 2   |            |            | -538.5092  | -512.4039  | -479.0583  | -438.3645  | -390.3449  |
| 1   |            | -212.4118  | -200.7862  | -183.5501  | -160.9711  | -133.4036  | -101.2238  |
| 2   |            |            | -177.3710  | -160.4629  | -137.6661  | -108.8531  | -73.9986   |
| 1   |            | -154.8206  | -140.1269  | -118.2691  | -89.4298   | -53.8527   | -11.9027   |
| <i>ortho</i> - $\text{H}_2\text{He}^+$ , dissociation limit 58.3124 $\text{cm}^{-1}$ : $\text{H}_2^+(v = 0, j = 1) + \text{He}$ |            |            |            |            |            |            |            |
| parity $e$  |            |            |            |            |            |            |            |
| $k$   | $J = 0$    | $J = 1$    | $J = 2$    | $J = 3$    | $J = 4$    | $J = 5$    | $J = 6$    |
| 0   | -1793.9093 | -1785.7450 | -1769.4254 | -1744.9683 | -1712.4008 | -1671.7590 | -1623.0884 |
| 1   |            | -1153.9249 | -1138.1849 | -1114.6224 | -1083.2960 | -1044.2872 | -997.7037  |
| 0   | -1062.2765 | -1054.9132 | -1040.1934 | -1018.1303 | -988.7427  | -952.0532  | -908.0861  |
| 0   | -657.8564  | -650.1900  | -634.8830  | -611.9896  | -581.5960  | -543.8286  | -498.8688  |
| 1   |            | -564.5792  | -555.6514  | -539.3139  | -516.2964  | -486.9120  | -451.4157  |
| 2   |            |            | -538.8675  | -514.1997  | -483.2973  | -446.3583  | -403.3916  |
| 0   | -537.5536  | -530.4963  | -516.2789  | -494.6767  | -465.3467  | -427.9695  | -382.5138  |
| 1   |            | -263.1765  | -252.2197  | -236.4432  | -216.0998  | -191.1843  | -161.6599  |
| 0   | -254.1435  | -248.6453  | -237.5731  | -221.0038  | -199.4074  | -173.4850  | -143.7602  |
| 0   | -189.9439  | -186.0880  | -176.8071  | -161.4668  | -139.9266  | -112.4335  | -79.6339   |
| 1   |            | -174.2914  | -159.5639  | -138.4376  | -110.7061  | -76.0767   | -34.5730   |
| 2   |            |            | -127.7872  | -110.4400  | -87.4584   | -58.9374   | -25.0044   |
| 1   |            | -68.8869   | -60.5497   | -48.3629   | -32.5161   | -13.1131   | 9.8467     |
| 0   | -48.2670   | -44.8744   | -38.1982   | -28.4248   | -15.7706   | -0.4739    | 17.2797    |
| 1   |            | -27.1164   | -15.6317   | -27.3970   | 1.6627     | 37.3617    | 55.6235    |
| 0   | 18.4100    | 22.3442    | 28.7083    | 0.9802     | 20.9859    | 40.5563    |            |
| 1   |            | 30.4736    | 36.4081    | 36.5138    | 45.6453    | 55.2153    |            |
| 0   | 39.5628    | 42.9216    | 49.2003    | 44.4892    | 54.0577    |            |            |
| 1   |            | 54.4848    | 56.6101    | 55.4116    |            |            |            |
| 0   | 55.6552    | 56.9079    | 58.2551    |            |            |            |            |
| parity $f$  |            |            |            |            |            |            |            |
| 1   |            | -1153.6077 | -1137.2268 | -1112.6860 | -1080.0223 | -1039.2852 | -990.5377  |
| 1   |            | -563.6444  | -553.6612  | -535.6203  | -510.2378  | -477.7349  | -438.2883  |
| 2   |            |            | -537.9399  | -511.6998  | -478.2236  | -437.4526  | -389.4213  |
| 1   |            | -262.8018  | -250.8828  | -233.3604  | -210.5984  | -182.9822  | -150.8663  |
| 1   |            | -175.9529  | -163.0626  | -143.4725  | -117.0023  | -83.6388   | -43.8879   |
| 2   |            |            | -127.8158  | -110.5865  | -87.9073   | -59.9876   | -26.9424   |
| 1   |            | -68.6670   | -59.9106   | -47.1821   | -30.8058   | -11.0218   | 12.1083    |
| 1   |            | -27.5906   | -16.9382   | -27.3987   | 1.6625     | 37.3375    |            |
| 1   |            | 29.9116    | 34.5573    | -1.1404    | 18.9917    | 40.8410    |            |
| 1   |            | 54.5926    | 56.3036    | 41.4620    | 50.5264    |            |            |

Table 2: Rovibrational energy levels of  $D_2He^+$  from CCVM calculations. The approximate quantum number  $k$  is the projection of  $J$  on the  $D_2^+-He$  axis  $R$ ; different values of  $k$  are mixed by Coriolis coupling. This mixing is stronger for the higher states.

| <i>ortho</i> - $D_2He^+$ , dissociation limit 0: $D_2^+(v = 0, j = 0) + He$ |            |            |            |            |            |            |            |
|---|------------|------------|------------|------------|------------|------------|------------|
| parity <i>e</i>   |            |            |            |            |            |            |            |
| <i>k</i>  | $J = 0$    | $J = 1$    | $J = 2$    | $J = 3$    | $J = 4$    | $J = 5$    | $J = 6$    |
| 0   | -1995.0221 | -1989.7727 | -1979.2772 | -1963.5420 | -1942.5767 | -1916.3942 | -1885.0108 |
| 1   |            | -1516.6690 | -1506.3547 | -1490.8943 | -1470.3012 | -1444.5934 | -1413.7936 |
| 0   | -1354.0790 | -1349.2223 | -1339.5127 | -1324.9580 | -1305.5699 | -1281.3638 | -1252.3591 |
| 0   | -1103.9373 | -1098.7694 | -1088.4414 | -1072.9688 | -1052.3752 | -1026.6926 | -995.9622  |
| 2   |            |            | -1048.2002 | -1032.8490 | -1012.3994 | -986.8678  | -956.2749  |
| 1   |            | -949.6101  | -940.2886  | -926.3205  | -907.7228  | -884.5185  | -856.7365  |
| 0   | -855.4376  | -850.9757  | -842.0563  | -828.6882  | -810.8843  | -788.6609  | -762.0379  |
| 1   |            | -700.6382  | -691.0112  | -676.5876  | -657.3904  | -633.4536  | -604.8249  |
| 0   | -677.5048  | -672.3690  | -662.1023  | -646.7142  | -626.2197  | -600.6393  | -570.0011  |
| 3   |            |            |            | -599.8370  | -581.2804  | -558.2580  | -530.9271  |
| 0   | -619.4238  | -614.7037  | -605.2811  | -591.1894  | -572.4721  | -549.1726  | -521.3158  |
| 2   |            |            | -572.4639  | -558.3276  | -539.5106  | -516.0391  | -487.9554  |
| 1   |            | -530.1485  | -521.9188  | -509.5557  | -493.0380  | -472.3365  | -447.4091  |
| 0   | -483.4875  | -479.4342  | -471.3280  | -459.1689  | -442.9550  | -422.6795  | -398.3285  |
| 0   | -382.0840  | -376.9896  | -366.8433  | -351.7335  | -331.8046  | -307.3234  | -280.5961  |
| 1   |            | -337.4361  | -334.5099  | -326.8758  | -315.3377  | -299.5276  | -277.2381  |
| 2   |            |            | -327.0282  | -311.7805  | -291.7210  | -267.1572  | -238.7637  |
| 0   | -311.6660  | -305.8144  | -294.9372  | -279.8648  | -261.1520  | -239.1468  | -214.0232  |
| 2   |            |            | -259.7601  | -254.7002  | -244.7032  | -230.5825  | -212.5540  |
| 1   |            | -247.1973  | -242.0733  | -236.7839  | -225.9174  | -211.2736  | -192.2673  |
| 3   |            |            |            | -228.1960  | -210.1158  | -189.2541  | -165.5287  |
| 0   | -238.0913  | -233.4300  | -224.6665  | -212.0132  | -195.3925  | -174.5212  | -149.2904  |
| 4   |            |            |            |            | -183.8732  | -156.5514  | -128.1776  |
| 0   | -199.9992  | -196.4549  | -189.3951  | -178.8909  | -165.0674  | -148.0976  | -124.7619  |
| 1   |            | -169.7211  | -159.7506  | -145.3737  | -128.7659  | -111.0052  | -90.9325   |
| 2   |            |            | -150.5716  | -139.1556  | -121.6659  | -97.3319   | -75.3754   |
| 0   | -137.6543  | -134.5506  | -128.3126  | -118.9386  | -106.5908  | -91.7577   | -67.5961   |
| 1   |            | -98.0431   | -92.0737   | -84.0973   | -74.1326   | -61.0169   | -43.9372   |
| 0   | -94.6518   | -92.6247   | -88.2092   | -80.4741   | -68.9474   | -54.3266   | -37.6237   |
| 2   |            |            | -86.1069   | -76.6360   | -63.8174   | -47.4573   | -26.7707   |
| 1   |            | -71.1694   | -65.6420   | -57.5612   | -46.9674   | -33.7098   | -17.5764   |
| 1   |            | -45.4923   | -37.4794   | -30.9719   | -24.5458   | -16.9425   | -8.0121    |
| 0   | -41.4540   | -39.5903   | -35.9310   | -25.4027   | -12.8509   | -0.4085    |            |
| 3   |            |            |            | -17.2467   | -10.5432   |            |            |
| 0   | -22.3532   | -20.1226   | -15.8690   | -10.0472   | -4.8349    |            |            |
| 0   | -6.2553    | -5.2991    | -3.5846    | -1.2003    |            |            |            |
| 4   |            |            |            |            | -3.3848    |            |            |
| 0   | -0.9668    | -0.2857    |            |            |            |            |            |
| 0   | -0.1169    |            |            |            |            |            |            |
| parity <i>f</i>   |            |            |            |            |            |            |            |
| 1   |            | -1516.5355 | -1505.9537 | -1490.0909 | -1468.9589 | -1442.5737 | -1410.9552 |
| 2   |            |            | -1048.2026 | -1032.8614 | -1012.4369 | -986.9560  | -956.4527  |
| 1   |            | -949.4136  | -939.6975  | -925.1332  | -905.7327  | -881.5116  | -852.4893  |
| 1   |            | -700.2484  | -689.8427  | -674.2530  | -653.5023  | -627.6222  | -596.6538  |
| 3   |            |            |            | -599.8346  | -581.2626  | -558.1831  | -530.6921  |
| 2   |            |            | -572.4646  | -558.3317  | -539.5257  | -516.0778  | -488.0266  |
| 1   |            | -529.8007  | -520.8790  | -507.4863  | -489.6093  | -467.2293  | -440.3205  |
| 2/1   |            |            | -330.8432  | -318.8783  | -302.8029  | -282.6791  | -258.5664  |
| 1/2   |            | -335.1855  | -324.7660  | -309.5642  | -289.6898  | -265.3987  | -237.2096  |
| 2   |            |            | -259.5189  | -254.0679  | -243.2481  | -227.5927  | -207.0277  |
| 3/1   |            |            |            | -232.9096  | -218.2846  | -200.6128  | -179.3465  |
| 1/3   |            | -245.3216  | -237.2610  | -223.4144  | -204.5902  | -181.7027  | -154.9819  |
| 4   |            |            |            |            | -183.8870  | -156.5705  | -124.7799  |
| 1   |            | -169.6786  | -159.6202  | -145.1664  | -128.6894  | -111.0092  | -90.9204   |
| 2   |            |            | -150.5633  | -139.0587  | -121.1920  | -96.4356   | -66.4402   |
| 1   |            | -97.7063   | -90.8449   | -80.8670   | -67.8617   | -52.1303   | -34.6110   |
| 2   |            |            | -86.1104   | -76.5926   | -63.7232   | -47.4427   | -27.0960   |
| 1   |            | -71.0678   | -65.2334   | -56.4480   | -44.5161   | -29.0851   | -9.7266    |
| 1   |            | -45.0902   | -36.1980   | -22.9868   | -12.8517   |            |            |
| 3   |            |            |            | -17.1834   | -6.2397    |            |            |
| 4   |            |            |            |            | -3.8015    |            |            |

continued

*para*-D<sub>2</sub>He<sup>+</sup>, dissociation limit 29.4092 cm<sup>-1</sup>: D<sub>2</sub><sup>+</sup>(*v* = 0, *j* = 1) + He

| parity <i>e</i> |              |              |              |              |              |              |              |
|-----------------|--------------|--------------|--------------|--------------|--------------|--------------|--------------|
| <i>k</i>        | <i>J</i> = 0 | <i>J</i> = 1 | <i>J</i> = 2 | <i>J</i> = 3 | <i>J</i> = 4 | <i>J</i> = 5 | <i>J</i> = 6 |
| 0               | -1995.0221   | -1989.7727   | -1979.2772   | -1963.5420   | -1942.5767   | -1916.3942   | -1885.0109   |
| 1               |              | -1516.6691   | -1506.3548   | -1490.8944   | -1470.3013   | -1444.5935   | -1413.7937   |
| 0               | -1354.0790   | -1349.2222   | -1339.5126   | -1324.9580   | -1305.5699   | -1281.3638   | -1252.3591   |
| 0               | -1103.9344   | -1098.7670   | -1088.4398   | -1072.9682   | -1052.3757   | -1026.6942   | -995.9646    |
| 2               |              |              | -1048.1989   | -1032.8483   | -1012.3993   | -986.8679    | -956.2750    |
| 1               |              | -949.6151    | -940.2917    | -926.3212    | -907.7210    | -884.5145    | -856.7312    |
| 0               | -855.4350    | -850.9734    | -842.0546    | -828.6872    | -810.8841    | -788.6614    | -762.0390    |
| 1               |              | -700.7546    | -691.0669    | -676.5691    | -657.3000    | -633.3099    | -604.6594    |
| 0               | -677.4620    | -672.3339    | -662.0807    | -646.7091    | -626.2301    | -600.6612    | -570.0280    |
| 3               |              |              |              | -599.8663    | -581.2798    | -558.2525    | -530.9465    |
| 0               | -618.9803    | -614.3166    | -604.9999    | -591.0481    | -572.4787    | -549.2979    | -521.4931    |
| 2               |              |              | -572.2231    | -558.1931    | -539.4519    | -515.9995    | -487.8743    |
| 1               |              | -530.4586    | -522.0794    | -509.5380    | -492.8575    | -472.0525    | -447.1121    |
| 0               | -483.3874    | -479.3507    | -471.2736    | -459.1488    | -442.9650    | -422.7072    | -398.3562    |
| 0               | -373.8092    | -369.8660    | -361.8472    | -349.5398    | -332.7356    | -311.2995    | -285.2030    |
| 1               |              | -348.8296    | -340.1571    | -326.8840    | -309.2554    | -287.8906    | -263.7827    |
| 2               |              |              | -320.6005    | -304.3300    | -284.3787    | -262.0074    | -237.5331    |
| 0               | -298.9760    | -295.8132    | -289.3869    | -279.4115    | -265.1799    | -245.3822    | -219.4627    |
| 3/2             |              |              |              | -251.8539    | -241.3644    | -225.9238    | -205.5897    |
| 2/3             |              |              | -254.3501    | -241.2252    | -227.0289    | -210.0001    | -190.0986    |
| 1               |              | -252.0377    | -240.8280    | -227.1402    | -210.9442    | -191.4041    | -167.9858    |
| 0               | -234.7883    | -230.8583    | -222.8221    | -210.4935    | -193.9968    | -173.6022    | -149.4335    |
| 4               |              |              |              |              | -181.7407    | -154.5074    | -122.8192    |
| 1               |              | -194.6516    | -187.0706    | -175.8354    | -161.0526    | -142.8278    | -121.2324    |
| 1               |              | -162.1476    | -152.6767    | -138.4157    | -119.4188    | -96.2313     | -72.9984     |
| 1               |              | -115.0155    | -110.5440    | -103.8982    | -94.8314     | -82.5356     | -63.0884     |
| 0               | -116.1312    | -112.6264    | -105.9378    | -96.3418     | -84.3498     | -70.5880     | -55.1555     |
| 3               |              |              |              | -93.6074     | -80.6222     | -64.2253     | -44.3454     |
| 0               | -92.6281     | -89.7260     | -83.8810     | -75.1400     | -63.5646     | -49.1575     | -32.0443     |
| 2               |              |              | -67.2018     | -56.5508     | -43.2575     | -28.3368     | -11.2081     |
| 0/1             | -72.7767     | -70.7329     | -64.0231     | -54.8286     | -42.4747     | -26.4694     | -7.6868      |
| 1/0             |              | -69.3838     | -60.9882     | -47.3677     | -28.8594     | -7.2580      | 12.7821      |
| 2               |              |              | -42.8938     | -33.5328     | -20.1733     | -1.0292      | 14.9488      |
| 1               |              | -21.4320     | -17.3961     | -11.4242     | -3.5288      | 6.2538       | 20.1412      |
| 3               |              |              |              | -7.2584      | 0.7089       | 7.6430       | 26.5976      |
| 0               | -13.7453     | -12.1959     | -9.1862      | -4.8452      | 11.0358      | 26.6657      |              |
| 1               |              | 1.3535       | 7.1043       | 14.3332      | 21.1633      |              |              |
| 0/1             | 16.6751      | 17.3402      | 19.6076      | 22.7282      | 26.0148      |              |              |
| 1/0             |              | 18.4618      | 21.1874      | 25.2904      |              |              |              |
| 1/0             |              | 27.3402      | 28.1537      | 29.1114      |              |              |              |
| 0/1             | 26.6910      | 28.2478      | 29.3445      |              |              |              |              |
| parity <i>f</i> |              |              |              |              |              |              |              |
| 1               |              | -1516.5356   | -1505.9538   | -1490.0910   | -1468.9590   | -1442.5738   | -1410.9553   |
| 2               |              |              | -1048.2014   | -1032.8609   | -1012.4373   | -986.9572    | -956.4546    |
| 1               |              | -949.4194    | -939.7027    | -925.1377    | -905.7363    | -881.5142    | -852.4908    |
| 1               |              | -700.3920    | -689.9734    | -674.3653    | -653.5920    | -627.6865    | -596.6914    |
| 3               |              |              |              | -599.8635    | -581.2596    | -558.1702    | -530.7013    |
| 2               |              |              | -572.2334    | -558.2409    | -539.5802    | -516.2557    | -488.2826    |
| 1               |              | -530.1651    | -521.1868    | -507.7187    | -489.7576    | -467.2961    | -440.3198    |
| 1               |              | -349.8114    | -342.8142    | -331.5706    | -315.8942    | -295.7604    | -271.2521    |
| 2               |              |              | -320.5937    | -304.0311    | -282.8609    | -257.3697    | -228.0515    |
| 3/2             |              |              |              | -252.5279    | -243.2243    | -229.6539    | -211.7034    |
| 2/3             |              |              | -254.4782    | -240.8455    | -225.6176    | -206.6407    | -183.8732    |
| 1               |              | -251.5912    | -239.2032    | -223.5438    | -204.7831    | -182.6063    | -156.7396    |
| 4               |              |              |              |              | -181.7481    | -154.5147    | -122.7532    |
| 1               |              | -194.5276    | -186.7114    | -175.1632    | -160.0491    | -141.5459    | -119.8308    |
| 1               |              | -161.9222    | -151.9965    | -137.0362    | -117.0321    | -92.2139     | -65.5319     |
| 1               |              | -114.3652    | -108.7563    | -100.5717    | -89.8754     | -76.4134     | -57.2112     |
| 3               |              |              |              | -93.5988     | -80.5846     | -64.1527     | -44.2571     |
| 2               |              |              | -67.2911     | -56.7261     | -43.2744     | -27.7342     | -10.8509     |
| 1               |              | -70.8379     | -62.7981     | -51.0121     | -35.7324     | -17.9346     | 1.0107       |
| 2               |              |              | -42.9583     | -33.8232     | -20.9170     | -3.2098      | 18.0102      |
| 1               |              | -21.5098     | -17.5903     | -11.7284     | -3.8875      | 6.1110       | 20.6678      |
| 3               |              |              |              | -7.2595      | 11.0208      | 27.0800      |              |
| 1               |              | 1.1218       | 6.6184       | 8 13.9143    | 21.1628      |              |              |
| 1               |              | 17.6248      | 20.1151      | 24.1565      | 29.3341      |              |              |
| 1               |              | 27.8931      | 28.6771      |              |              |              |              |

dipole function over the BF basis is given in the Appendix of Ref. [53], here it simply contains products of Wigner 3- $j$  symbols. Replacing the center-of-mass coordinates and the basis of  $\text{H}_2\text{He}^+$  by those of  $\text{D}_2\text{He}^+$  yields the dipole function of  $\text{D}_2\text{He}^+$ . Finally, we generated theoretical line lists for both  $\text{H}_2\text{He}^+$  and  $\text{D}_2\text{He}^+$  by computing the frequencies and dipole transition moments for all allowed transitions between the calculated bound rovibrational eigenstates.

### 3.5. Rovibrational energy levels and transitions

The rovibrational energy levels of  $\text{H}_2\text{He}^+$  and  $\text{D}_2\text{He}^+$ , obtained by the CCVM method, are listed in Tables 1 and 2, respectively. The levels from the  $\text{D}^2\text{FOPI}$  calculations calculated on the same 3D potential surface all agree with these levels to better than  $0.5\text{ cm}^{-1}$ . This holds even for levels close to the dissociation limit, which nicely confirms that both calculations are correct and precise. The first phenomenon one can observe in these tables is that the lower levels of *para*- $\text{H}_2\text{He}^+$  and those of *ortho*- $\text{H}_2\text{He}^+$  have almost the same energies, just as the lower levels of *ortho*- $\text{D}_2\text{He}^+$  and those of *para*- $\text{D}_2\text{He}^+$ . This indicates that in their lower rovibrational states the complexes are quite rigid. The levels above about  $-500\text{ cm}^{-1}$  become less similar for the *para* and *ortho* species; their energies differ more and more when they get closer to the dissociation limit. The second observation is that the spacings between the levels with increasing values of  $J$ , *i.e.*, the corresponding rotational constants, become smaller with increasing energy. This implies that the higher states become more and more diffuse or, in other words, that the average distance  $R$  between the subunits increases with the energy. Other points worth mentioning are that  $\text{D}_2\text{He}^+$  has a substantially smaller zero-point energy, *i.e.*, a larger  $D_0$  value, than  $\text{H}_2\text{He}^+$  and that  $\text{D}_2\text{He}^+$  has many more bound rovibrational states than  $\text{H}_2\text{He}^+$ .

Among the states in Tables 1 and 2 one may distinguish the three fundamental excitations in the modes  $\nu_1 \equiv \nu_r$ ,  $\nu_2 \equiv \nu_b$ , and  $\nu_3 \equiv \nu_s$ . The  $\nu_1 = 1$  excited state lies above the dissociation limit of *para*- $\text{H}_2\text{He}^+$ , it is probably a resonance, but it is a bound state in *ortho*- $\text{H}_2\text{He}^+$ , because of its larger  $D_0$  value. Actually we find two states with a substantial amount of H-H stretch character, at energies  $18.4$  and  $39.6\text{ cm}^{-1}$  for  $J = 0$ . The band origins of the excitations to these states from the ground state are  $1812.3$  and  $1833.5\text{ cm}^{-1}$ . There are two of them because the H-H stretch mode couples with the bend and stretch modes of the  $\text{H}_2\text{He}^+$  ion. In the  $\text{D}_2\text{He}^+$  ion only a single state has dominant D-D stretch character, at  $-677.5\text{ cm}^{-1}$  for  $J = 0$ , which corresponds to a band origin of  $1317.5\text{ cm}^{-1}$ . As one will see below, this is reflected in the experimental spectra by the width and shape of the corresponding peaks in the  $\text{H}_2\text{He}^+$  and  $\text{D}_2\text{He}^+$  spectra.

The bend fundamental mode ( $\nu_2 = 1$ ) in a linear triatomic molecule is degenerate and has a vibrational angular momentum  $l_{\nu_2} = \pm 1$ . In Table 1 this excited state is at  $-1153.9\text{ cm}^{-1}$  for  $\text{H}_2\text{He}^+$  and has a projection angular momentum  $k = 1$  that corresponds with these  $l_{\nu_2}$  values. The  $\nu_2$  excitation energy is thus  $640.0\text{ cm}^{-1}$ . Table 2 shows that the bend excited state in  $\text{D}_2\text{He}^+$  has an energy of  $-1516.6\text{ cm}^{-1}$  and this corresponds to an excitation energy of  $478.4\text{ cm}^{-1}$ .

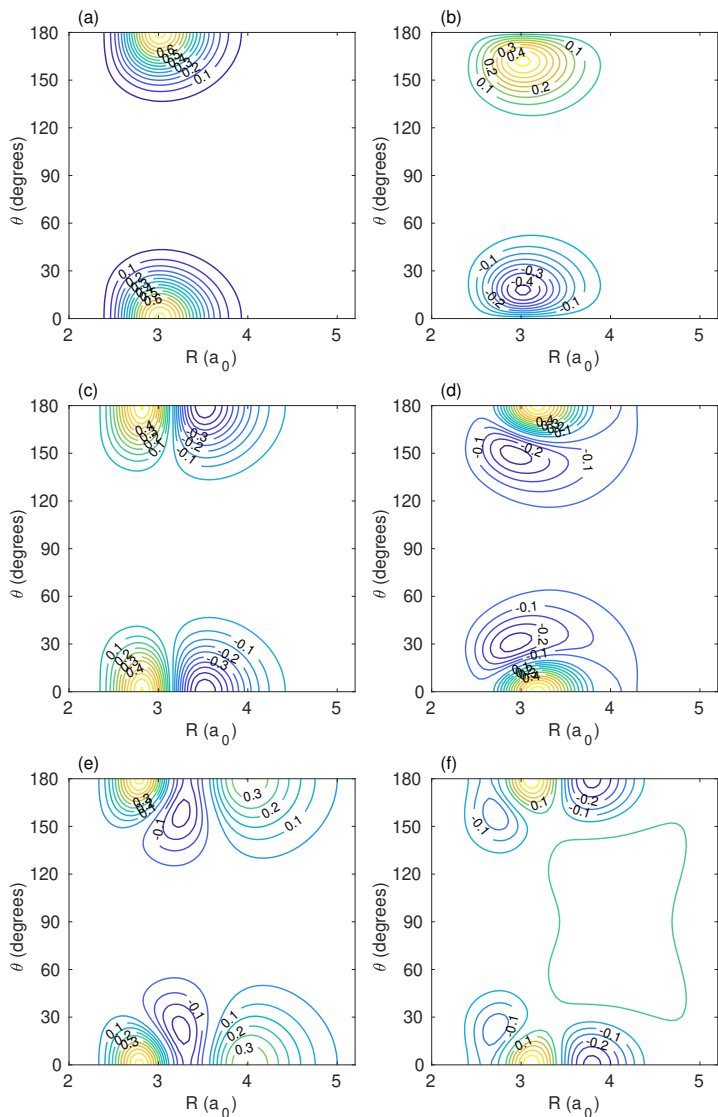


Figure 5: Wave-function contour plots of some states in *para*- $\text{H}_2\text{He}^+$  with the H-H distance fixed at  $r = 2.1 a_0$ . Panel (a) shows the ground  $J = 0$  state at energy  $-1793.9\text{ cm}^{-1}$ , panel (b) the  $\nu_2 = 1$  bend excited state with  $k = J = 1$  at  $-1153.9\text{ cm}^{-1}$ , panel (c) the  $\nu_3 = 1$   $\text{H}_2^+$ -He stretch excited state with  $J = 0$  at  $-1062.3\text{ cm}^{-1}$ , panel (d) the  $\nu_2 = 2$  bend overtone state with  $J = k = 0$  at  $-659.8\text{ cm}^{-1}$ , panel (e) the  $\nu_3 = 2$  stretch overtone state with  $J = 0$  at  $-538.3\text{ cm}^{-1}$ , and panel (f) the  $J = 0$  state at  $-300.6\text{ cm}^{-1}$ .

The  $\nu_3 = 1$  state excited in the  $\text{H}_2^+$ -He stretch mode lies at  $-1062.3\text{ cm}^{-1}$  in  $\text{H}_2\text{He}^+$  and the corresponding fundamental excitation energy is  $731.6\text{ cm}^{-1}$ . In  $\text{D}_2\text{He}^+$ , the  $\text{D}_2^+$ -He excited state lies at  $-1354.1\text{ cm}^{-1}$  and the  $\nu_3 = 1$  band origin is at  $640.9\text{ cm}^{-1}$ .

A bend overtone ( $\nu_2 = 2$ ) and a stretch overtone ( $\nu_3 = 2$ ) state of  $\text{H}_2\text{He}^+$  can also be found in Table 1. The bend overtone level with  $l_{\nu_2} = 0$  at  $-659.8\text{ cm}^{-1}$  and the stretch overtone level at  $-538.3\text{ cm}^{-1}$ , both for  $J = 0$ , correspond to band origins of  $1134.1$  and  $1255.6\text{ cm}^{-1}$ , respectively. The corresponding  $J = 0$  overtone levels of  $\text{D}_2\text{He}^+$  in Table 2 are at  $-1103.8$  and  $-855.4\text{ cm}^{-1}$ , which corresponds to band origins of  $891.1$  and  $1139.6\text{ cm}^{-1}$ , respectively.

The character of these states is illustrated in the wavefunction contour plots of Fig. 5. They are displayed for *para*-H<sub>2</sub>He<sup>+</sup>, but are very similar for *ortho*-H<sub>2</sub>He<sup>+</sup>, except that for the latter system they have a node determined by symmetry at  $\theta = 90^\circ$ . For D<sub>2</sub>He<sup>+</sup> they are qualitatively similar. The plot in Fig. 5(a) shows that the ground state is quite well localized in the region of the two equivalent minima of the PES. The wave function has equal amplitude and the same sign in the minima for *para*-H<sub>2</sub>He<sup>+</sup>, and opposite sign (not shown) for *ortho*-H<sub>2</sub>He<sup>+</sup>. It has a negligible amplitude between the two minima, however, which shows that there is practically no tunneling between the structures localized at the two minima. Figure 5(b), for the  $\nu_2 = 1$  bend excited state with  $l_{\nu_2} = k = 1$ , clearly confirms the character of this state, it has a nodal plane in the angular coordinate at the linear structures with  $\theta = 0^\circ$  and  $180^\circ$ . Figure 5(c) for the  $\nu_3 = 1$  H<sub>2</sub><sup>+</sup>-He stretch excited state has a node in the radial coordinate  $R$ , which also confirms our assignment. Figure 5(d) and 5(e) show the  $\nu_2 = 2$  bend and  $\nu_3 = 2$  stretch overtone states, respectively. Finally, Fig. 5(f) corresponds to a higher excited state at  $-300.6$  cm<sup>-1</sup>. It illustrates that, indeed, the higher states are more delocalized and extend to larger H<sub>2</sub><sup>+</sup>-He distances  $R$ . The non-negligible amplitude at  $\theta = 90^\circ$  suggests that tunneling between the two minima is appreciable. Some further comments on the energy levels and the transitions between them are made below, when we discuss the experimental spectra and their comparison with theory.

The frequencies and line strengths of all dipole-allowed transitions between these energy levels of H<sub>2</sub>He<sup>+</sup> and D<sub>2</sub>He<sup>+</sup> are given in the Supplementary Material. The dipole transition moments and line strengths were calculated from the wave functions of the corresponding states and the *ab initio* dipole moment function described in Section 3.4.

#### 4. Low-Resolution Spectroscopy of H<sub>2</sub>He<sup>+</sup>

The experimental spectrum obtained for H<sub>2</sub>He<sup>+</sup> is shown in Fig. 6, together with a simulated spectrum based on the line lists from the variational calculations. The D<sup>2</sup>FOPI and CCVM calculations yield indistinguishable spectra. As we used *n*-H<sub>2</sub> as a precursor in the ion source, we assume that its *o/p* ratio of 3:1 is transferred to the *o/p* ratio of H<sub>2</sub>He<sup>+</sup> generated in the ion trap. At the cryogenic conditions of the experiment all transitions originate from the lowest quantum levels of *o/p*-H<sub>2</sub>He<sup>+</sup>. At an assumed rotational temperature of about 15 K (due to known heating effects [54, 55], the rotational and translational temperatures of the ions are higher than the nominal temperature of the trap, 4 K), only the lowest three levels with  $J = 0, 1$ , and 2 of *o/p*-H<sub>2</sub>He<sup>+</sup> are occupied (in total six levels). Starting from these six levels, the FELIX laser has probed spectral features of H<sub>2</sub>He<sup>+</sup> in the range of 540–1900 cm<sup>-1</sup>. Most of these features, being below the dissociation limits of  $D_0 = 1794$  cm<sup>-1</sup> for *para*-H<sub>2</sub>He<sup>+</sup> and  $D_0 = 1852$  cm<sup>-1</sup> for *ortho*-H<sub>2</sub>He<sup>+</sup>, must be due to multi-photon processes (the limits are indicated by vertical dashed lines in Fig. 6). The appearance or non-appearance of spectral features, in comparison to the predictions provided by the variational calculations, depends on the availability of

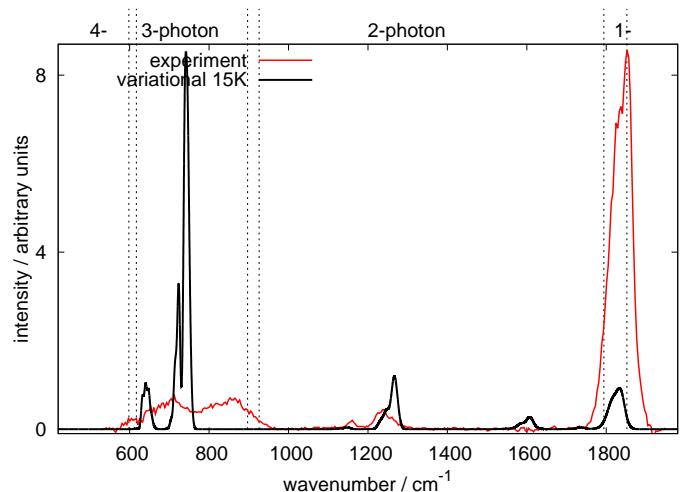


Figure 6: IR spectrum of H<sub>2</sub>He<sup>+</sup> (red), recorded by counting the number of H<sub>2</sub>He<sup>+</sup> ions (mass 6 u) as a function of the FELIX wavenumber (cm<sup>-1</sup>), and the theoretical spectrum (black) at 15 K obtained with the line lists (transition frequencies and line strengths) from the variational calculations. The ions have been trapped and exposed to the pulsed radiation for 2.5 s. The dissociation limit at  $D_0 = 1794$  cm<sup>-1</sup> for the *para* species and  $D_0 = 1852$  cm<sup>-1</sup> for the *ortho* species, as well as  $D_0/2$  and  $D_0/3$ , are indicated by vertical dashed lines, providing the number of photons necessary for the detected dissociation process. The strong peak at  $1840$  cm<sup>-1</sup> is caused by IR-active transitions into states with considerable H-H stretch character. Further probable assignments as well as the resemblance of and differences between the experimental and theoretical spectra are explained in the text.

intermediate resonant states, as well as on experimental parameters such as the spectral width of the FELIX frequency (typically 0.5 %) and the focusing of the beam in the trap.

The most prominent peak in Fig. 6 is the one around  $1840$  cm<sup>-1</sup>, which lies just below the dissociation limit of *ortho*-

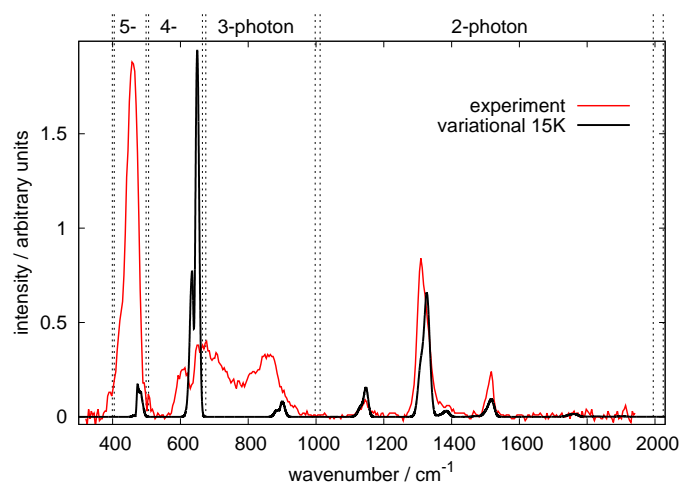


Figure 7: IR spectrum of D<sub>2</sub>He<sup>+</sup> (red), recorded by counting the number of D<sub>2</sub>He<sup>+</sup> ions (mass 8 u) as a function of FELIX wavenumber (cm<sup>-1</sup>) and the theoretical spectrum (black) at 15 K obtained with the line lists from the variational calculations. The ions have been trapped and exposed to the pulsed radiation for 2.5 s. The dissociation limits at  $D_0 = 1995$  and  $2024$  cm<sup>-1</sup> as well as  $D_0/2$ ,  $D_0/3$ , etc. are indicated by vertical dashed lines. The good agreement between the measured and theoretical spectra allows the assignment of all experimental features, see the summary in Table 3. In particular, the strong band at  $1309$  cm<sup>-1</sup> is identified as the fundamental D-D stretch.

Table 3: Measured and calculated vibrational transition frequencies (in  $\text{cm}^{-1}$ ) and some assignments for the molecular ions  $\text{H}_2\text{He}^+$  and  $\text{D}_2\text{He}^+$ . The experimental uncertainties of the FELIX data presented in this table are typically 0.5 %. Due to the low temperature, all transitions start at  $(v'_r v'_b v'_s) = (000)$ , with  $k'' = 0$  and  $J'' < 4$ .

| molecule                                  |      | this work         |             |                          | previous <i>ab initio</i> results |                   |                   |                   |                     |
|---|------|-------------------|-------------|--------------------------|-----------------------------------|-------------------|-------------------|-------------------|---------------------|
| $(v'_r v'_b v'_s)$                        | $k'$ | expt.             | VPT2(harm.) | variational <sup>a</sup> | [25] <sup>a</sup>                 | [18] <sup>b</sup> | [16] <sup>b</sup> | [15] <sup>b</sup> | [14] <sup>b,c</sup> |
| <b><math>\text{H}_2\text{He}^+</math></b> |      |                   |             |                          |                                   |                   |                   |                   |                     |
| (0 1 0)                                   | 1    | 695 <sup>d</sup>  | 648(721)    | 640.0 [640.0]            | 647.5 [647.5]                     | 646               | 643               | 643               | 472                 |
| (0 0 1)                                   | 0    | 840 <sup>d</sup>  | 745(988)    | 731.6 [731.6]            | 733.7 [733.7]                     | 716               | 718               | 718               | 732                 |
| (0 2 0)                                   | 0    | 1159              | 1258        | 1136.1 [1134.1]          | 1151.8 [1150.1]                   |                   | 1136              | 1137              | 960                 |
| (0 0 2)                                   | 0    | 1234 <sup>e</sup> | 1280        | 1256.4 [1255.6]          | 1264.2 [1263.6]                   |                   | 1231              | 1231              | 1331                |
| – <i>f</i>                                | 0    | –                 | –           | 1604                     | 1621                              |                   |                   |                   |                     |
| (1 0 0) <sup>g</sup>                      | 0    | 1840              | 1834(1937)  | 1812/1833                | 1809/1832                         | 1825              |                   | 1844              |                     |
| <b><math>\text{D}_2\text{He}^+</math></b> |      |                   |             |                          |                                   |                   |                   |                   |                     |
| (0 1 0)                                   | 1    | 459               | 481         | 478.4 [478.4]            |                                   |                   |                   | 481               | 325                 |
| (0 0 1)                                   | 0    | 670 <sup>d</sup>  | 644         | 640.9 [640.9]            |                                   |                   |                   | 630               | 610                 |
| (0 2 0)                                   | 0    | 860 <sup>d</sup>  | 943         | 891.1 [891.1]            |                                   |                   |                   | 897               | 695                 |
| (0 0 2)                                   | 0    | 1145              | 1175        | 1139.6 [1139.6]          |                                   |                   |                   | 1117              | 1142                |
| (1 0 0)                                   | 0    | 1309              | 1299        | 1317.5 [1317.6]          |                                   |                   |                   | 1326              | 1420                |
| – <i>f</i>                                | 0    | 1385 <sup>h</sup> | –           | 1375.6 [1376.0]          |                                   |                   |                   |                   |                     |
| – <i>f</i>                                | 0    | 1516              | –           | 1511.5 [1511.6]          |                                   |                   |                   |                   |                     |

<sup>a</sup> The levels shown correspond to *ortho*- $\text{H}_2\text{He}^+$ . Their *para* counterparts are presented in brackets where pairing is straightforward.

<sup>b</sup> The results of previous *ab initio* calculations have been averaged for *ortho/para* species and rounded.

<sup>c</sup> Calculation of Ref. [14] performed on early unreliable PES. Significant deviations.

<sup>d</sup> Due to multi-photon process, experimental signal is very broad, shifted and unspecific (see also text). Assignment of experimental signal is therefore tentative.

<sup>e</sup> Feature has shoulder on the blue side at about  $1261 \text{ cm}^{-1}$  which might be associated with the theoretical predictions

<sup>f</sup> Delocalized upper state that cannot be attributed to a specific quantum number

<sup>g</sup> The variational results assign this feature to *o*- $\text{H}_2\text{He}^+$ . It has H–H stretch character with two components including He-stretch and bend motions of the complex (see also text).

<sup>h</sup> Experimental signal appears as a small blue shoulder to the D–D-stretch.

$\text{H}_2\text{He}^+$ . It has a clearly discernible shoulder at about  $20\text{ cm}^{-1}$  to the lower wavenumber side, a separation that is larger than the FELIX bandwidth. The observed feature nicely agrees with the simulated peak from the variational calculations, which has a similar shoulder. In fact, the variational calculations predict two  $J = 0$  states at  $18.4$  and  $39.6\text{ cm}^{-1}$  in *ortho*- $\text{H}_2\text{He}^+$  with considerable  $\text{H}_2^+$  stretch character. They give rise to excitations from the ground state with band origins at  $1812$  and  $1833\text{ cm}^{-1}$ . The VPT2 calculation predicts a  $\nu_1 = 0 \rightarrow 1$  transition at  $1837\text{ cm}^{-1}$ . The experimental uncertainty is at least  $9\text{ cm}^{-1}$ , so the calculations agree very well with experiment and suggest that the broad peak around  $1840\text{ cm}^{-1}$  indeed corresponds to excitation of the  $\text{H}_2^+$  stretch mode, while the two components originate from its coupling to the stretch and bend motions of the complex. It is also possible that resonances beyond the dissociation limit in *para*- $\text{H}_2\text{He}^+$  (not taken into account in the variational calculations) contribute to this peak. As further explained in the Conclusions and Outlook section, high-resolution studies are needed to resolve the details.

In the two-photon region, between about  $900$  and  $1800\text{ cm}^{-1}$ , only two weak spectral features, at  $1159\text{ cm}^{-1}$  and at  $1234\text{ cm}^{-1}$  (with a blue shoulder at about  $1261\text{ cm}^{-1}$ ) are discernible. These transitions are weak as they are not fundamentals, and because the dissociation via a second photon leading to a near-resonant or virtual state near  $2400\text{ cm}^{-1}$  seems ineffective. By comparison to theory (see black simulation in Fig. 6), these features are identified as transitions to the bend overtone ( $\nu_2 = 2$ ) and stretch overtone ( $\nu_3 = 2$ ), with theoretical band origins at  $1133.1$  and  $1255.6\text{ cm}^{-1}$ , respectively, see Section 3.5. Another peak at a somewhat higher wavenumber, about  $1600\text{ cm}^{-1}$ , which is not observed in the experiment, is predicted by theory to originate from a transition to a level at  $-189.9$  (for  $J = 0$ ) of *ortho*- $\text{H}_2\text{He}^+$  which corresponds to a delocalized state and therefore has a rather different energy in *para*- $\text{H}_2\text{He}^+$ . The experimental and theoretical results are summarized in Table 3, where we provide the most probable assignments of the experimental features, as well.

Finally, there are two wide and unspecific experimental features in the three-photon region below  $900\text{ cm}^{-1}$ . The two strong peaks predicted by theory in this region have band origins at  $632$  and  $732\text{ cm}^{-1}$  and correspond to the bend ( $\nu_2 = 0 \rightarrow 1$ ) and stretch ( $\nu_3 = 0 \rightarrow 1$ ) fundamentals. So the observed features in the experimental spectrum must be related to these fundamental transitions. The extent of the observed broadening and shifting effect remains puzzling, though such effects are known in multi-photon spectroscopy while the spectral features should be narrower in the case of multiple photon absorption as the profile is governed by the absorption of the first photon. The key in understanding the observed multi-photon phenomenon lies in the high absorption intensity of these fundamental modes (see the spectroscopic simulations) together with the high power of FELIX at these low frequencies, as well as the near-proximity of resonant states for the multi-photon process. The high intensity and the Lorentzian line-shape of the transform-limited band pass of the light source can lead to very broad absorption features which are difficult to separate from background fluctuations. These effects become more

and more pronounced when the number of photons increases. This is clearly the case for the 3-photon region of the spectrum shown in Fig. 6. In fact, the complete region shows some kind of absorption. One might argue that at least the peaks should be much more pronounced and coincide with the theoretical peaks, if those predictions were right. However, while the absorption of the first photon is predicted much more intense, the actual features are substantially smaller than the main feature at  $1840\text{ cm}^{-1}$ . Instead these 3-photon bands are only pulled out of the background because of the large absorption of the first photon, such that an off-resonance absorption is observed. As a result, the spectral features are blurred and a proper assignment is difficult. This effect is also observed for the  $\text{D}_2\text{He}^+$  spectrum as will be discussed below.

## 5. Low-Resolution Spectroscopy of $\text{D}_2\text{He}^+$

The spectrum measured for  $\text{D}_2\text{He}^+$  is shown in Fig. 7, again in combination with the spectrum simulated with the theoretically calculated line lists. Here again, for the same reason, only the CCVM spectrum is shown. We assume the *o/p*-ratio of  $\text{D}_2\text{He}^+$  to be 2:1, while only the lowest  $J = 0, 1, 2$ , and 3 levels are substantially populated at an assumed rotational temperature of  $15\text{ K}$ . Due to the lower wavenumbers of the fundamental vibrational modes and the correspondingly lower zero-point energy, the PES can host significantly more rovibrational states for  $\text{D}_2\text{He}^+$ . This leads to a higher density of states which may be beneficial for the multi-photon detection process. The smaller zero-point energy results in dissociation thresholds for  $\text{D}_2\text{He}^+$  that are higher than for  $\text{H}_2\text{He}^+$  and are calculated to be  $D_0 = 1995\text{ cm}^{-1}$  for *ortho*- $\text{D}_2\text{He}^+$  and  $D_0 = 2024\text{ cm}^{-1}$  for *para*- $\text{D}_2\text{He}^+$ . They are again marked by dashed vertical lines in Fig. 7.

A prominent and well-defined peak in the experimental  $\text{D}_2\text{He}^+$  spectrum is the one at  $1309\text{ cm}^{-1}$  in the 2-photon region. It is identified as the D–D stretch ( $\nu_1 = 0 \rightarrow 1$ ) transition, which was first reliably predicted to be at  $1326.1\text{ cm}^{-1}$  by Špirko and Kraemer 25 years ago [15]. Our variational calculations predict the D–D stretch band origin at  $1317\text{ cm}^{-1}$ . Given the experimental uncertainty of at about  $6\text{ cm}^{-1}$  in this frequency region, this agrees well with experiment. In clear contrast with  $\text{H}_2\text{He}^+$ , where we found two states with strong H–H stretch character, only a single vibrational state of  $\text{D}_2\text{He}^+$  has substantial D–D stretch character. This is reflected by the peak in Fig. 7 being narrower than the corresponding peak in the  $\text{H}_2\text{He}^+$  spectrum in Fig. 6 and by the absence of the shoulder that was found in the latter peak.

Additional peaks in the two-photon region of the spectrum in Fig. 7 are found at  $1145$ ,  $1385$ , and  $1516\text{ cm}^{-1}$ . They all agree with peaks in the simulated theoretical spectra, but only the transition at  $1145\text{ cm}^{-1}$  can be simply assigned as the  $\text{D}_2^+$ –He stretch overtone transition ( $\nu_3 = 0 \rightarrow 2$ ) with a predicted band origin of  $1140\text{ cm}^{-1}$ , while the others involve transitions to higher, more delocalized states that cannot be attributed to specific quantum numbers. Table 3 gives an overview of the peaks and their assignment.

The peak most intense and lowest in wavenumber is the one at about  $459\text{ cm}^{-1}$ . Špirko and Kraemer [15] predicted a peak at  $481.2\text{ cm}^{-1}$ , while our variational calculations predict a peak at  $473\text{ cm}^{-1}$ , due to the bend fundamental ( $\nu_2 = 0 \rightarrow 1$ ) transition. Probably due to the multi-photon process (about five photons are necessary for dissociation), the experimental peak is red-shifted compared to the theoretical predictions. The very high intensity and compactness of this peak seems to be caused by an accidentally favourable multi-photon ladder.

Furthermore, a much broader feature is found between  $550$  and  $950\text{ cm}^{-1}$ , *i.e.*, in the region where theory predicts transitions at  $641$  and  $891\text{ cm}^{-1}$  that are due to the stretch fundamental ( $\nu_3 = 0 \rightarrow 1$ ) and bend overtone ( $\nu_2 = 0 \rightarrow 2$ ) transitions, respectively. Similar to the  $\text{H}_2\text{He}^+$  case, the  $\text{D}_2\text{He}^+$  experimental spectrum suffers from substantial broadening and shifting effects when three or more photons are absorbed simultaneously, rendering the assignment of the experimental features challenging.

## 6. Conclusions and Outlook

Using a combination of a cryogenic ion trap machine with a highly tunable and powerful pulsed IR source a number of IR vibrational modes of the fundamental molecules  $\text{H}_2\text{He}^+$  and  $\text{D}_2\text{He}^+$  have been identified experimentally at low resolution. The measurements are supplemented with high-level *ab initio* electronic structure and first-principles nuclear-motion computations of the rovibrational states and transitions for both ions. Unfortunately, due to the detection *via* multi-photon dissociation, not all vibrational states predicted by theory to be intense could be detected, and some low-frequency features exhibit strong broadening and shifting. Nevertheless, the important IR active and bright H–H and D–D stretches of  $\text{H}_2\text{He}^+$  and  $\text{D}_2\text{He}^+$  have been observed, and confirmed by theory, at  $1840(9)$  and  $1309(6)\text{ cm}^{-1}$ , respectively. Furthermore, bands due to the fundamental and overtone transitions of the  $\text{H}_2^+-\text{He}$  and  $\text{D}_2^+-\text{He}$  bend and stretch modes have been observed and theoretically identified, as well as transitions to higher and more delocalized rovibrational states of these complexes that cannot be assigned to specific quantum numbers.

This work enables follow-up high-resolution IR spectroscopic investigations, very similar to the stepwise pathway we are following for the proton-helium complexes  $\text{HHe}_n^+$  [35, 36, 37]. The accurate calculations of the rovibrational states of  $\text{H}_2\text{He}^+$  and  $\text{D}_2\text{He}^+$  presented here will greatly help in the interpretation of these more detailed spectra. Prime targets of this endeavour will be the mentioned H–H and D–D stretches. These can be conveniently investigated at high resolution using powerful quantum cascade lasers. For the H–H feature at  $1840(9)\text{ cm}^{-1}$  we hope to resolve the two theoretically predicted underlying *ortho*- $\text{H}_2\text{He}^+$  bands. As these are below the corresponding dissociation limit, narrow rovibrational lines can be expected, but a second photon will be needed to finally dissociate the molecule. A similar approach may be applied to the D–D stretch at  $1309(6)\text{ cm}^{-1}$ . In order to explore the interesting low-frequency fundamental bands heavily blurred in

this work, double-resonance experiments at much lower intensities should be carried out. As an example, the wavenumber of FELIX could be kept fixed at the 2-photon feature of  $\text{D}_2\text{He}^+$  at  $1309\text{ cm}^{-1}$  while scanning a high-resolution laser across the low-frequency bands.

Once the IR spectra are known to spectroscopic accuracy, the ground vibrational state can be investigated in detail. Rotational spectroscopy of  $\text{H}_2\text{He}^+$  and  $\text{D}_2\text{He}^+$  is feasible as they possess large permanent dipole moments in their ground vibrational state; Meuwly and Hutson [19] predicted a value of  $5.1\text{ D}$  for  $\text{H}_2\text{He}^+$ . We find the permanent dipole moment of  $\text{H}_2\text{He}^+$  at its equilibrium geometry to be  $3.46\text{ D}$  and the ground-state average value to be  $3.76\text{ D}$ . The corresponding values for  $\text{D}_2\text{He}^+$  are  $2.20$  and  $2.41\text{ D}$ , respectively. At the low temperatures prevailing in the trap experiment, the spectrum should resemble that of a simple linear rotor, with the transitions  $J = 1 \leftarrow 0$  (at about  $8.164\text{ cm}^{-1} = 244.7\text{ GHz}$  for both *ortho* and *para*- $\text{H}_2\text{He}^+$ ) and  $2 \leftarrow 1$  (at about  $16.319\text{ cm}^{-1} = 489.2\text{ GHz}$  for both *ortho* and *para*) being prime targets. While *ortho*- and *para*- $\text{H}_2\text{He}^+$  have thus very similar transition frequencies for low-lying states (the degeneracy of the *ortho* and *para* states is lifted by quantum statistics), we expect the *para* transitions to exhibit only fine structure, with a doublet caused by the electronic spin  $S = 1/2$ , whereas *ortho* transitions have additional hyperfine structure. At the current level of theory and convergence, the variational computations predict a difference between the low-lying *ortho* and *para*-transitions on the order of MHz, which can be resolved in a high-resolution experiment, and give some important hints to the magnitude of the corresponding tunneling splittings. For *ortho*- $\text{D}_2\text{He}^+$ , the corresponding rotational transitions are predicted to be at  $5.249\text{ cm}^{-1} = 157.3\text{ GHz}$  ( $J = 1 \leftarrow 0$ ) and  $10.496\text{ cm}^{-1} = 314.7\text{ GHz}$  ( $J = 2 \leftarrow 1$ ). Rotational spectroscopy of these lines can be done by combining high-resolution IR dissociation with a rotational transition in a double-resonance scheme, as recently demonstrated for the complexes  $\text{CH}_3^+-\text{He}$  and  $\text{HCO}^+-\text{He}$  [56, 57]. Alternatively, a direct rotational spectroscopy scheme with one single mm-wave rotational photon may be applied [58, 59, 60, 61], hindering the attachment of a second He atom to form  $\text{H}_2\text{He}_2^+$  (or  $\text{D}_2\text{He}_2^+$ ).

Another interesting pathway to follow are studies of larger complexes of the form  $\text{H}_2\text{He}_n^+$  and their isotopic variants.  $\text{H}_2\text{He}_2^+$ , for instance, has been predicted to have a linear symmetric structure [62], and we calculated the dissociation for the loss of one He atom to be on the order of only  $D_0 = 380\text{ cm}^{-1}$ . In the course of this work we started to investigate  $\text{H}_2\text{He}_2^+$  and  $\text{D}_2\text{He}_2^+$ , the full results of which will be published elsewhere. The first results seem to indicate the H–H stretch in  $\text{H}_2\text{He}_2^+$  to be IR inactive, being a confirmation of  $\text{H}_2\text{He}_2^+$  to be linear and symmetric (in addition to the mass spectrum in Fig. 2 showing  $\text{H}_2^+$  to attach only two He atoms). It remains an interesting question whether  $\text{H}_2\text{He}_2^+$  at higher vibrational excitation should be considered as a symmetric molecule or rather as a solvated  $\text{H}_2\text{He}^+-\text{He}$  complex.

## Acknowledgements

We acknowledge the support of Radboud University and of the Nederlandse Organisatie voor Wetenschappelijk Onderzoek (NWO), providing the required beam time at the FELIX Laboratory. We highly appreciate the skillful assistance of the FELIX staff. The research leading to the results presented has been supported by the project CALIPSOplus under the Grant Agreement 730872 from the EU Framework Programme for Research and Innovation HORIZON 2020. The German co-authors have been supported by the Deutsche Forschungsgemeinschaft (DFG) via SFB 956 (project ID 184018867) and grants AS 319/2-2 and SCHL 341/6-2. The Hungarian co-authors are grateful to NKFIH for generous support (grant no. K119658 and FK134291). The work in Budapest was also supported by the János Bolyai Research Scholarship of the Hungarian Academy of Sciences and by the ELTE Institutional Excellence Program (TKP2020-IKA-05) financed by the Hungarian Ministry of Human Capacities.

## References

- [1] T. R. Hogness, E. G. Lunn, The ionization of hydrogen by electron impact as interpreted by positive ray analysis, *Phys. Rev.* 26 (1925) 44–55.
- [2] T. M. Kojima, N. Kobayashi, Y. Kaneko, Formation of helium cluster ions  $\text{HHe}_x^+$  ( $x \leq 14$ ) and  $\text{H}_3\text{He}_x^+$  ( $x \leq 13$ ) in a very low temperature drift tube, *Z. Phys. D* 23 (1992) 181–185.
- [3] P. Bartl, C. Leidlmair, S. Denifl, P. Scheier, O. Echt, Cationic complexes of hydrogen with helium, *ChemPhysChem* 14 (2013) 227–232.
- [4] R. Güsten, H. Wiesemeyer, D. Neufeld, K. M. Menten, U. U. Graf, K. Jacobs, B. Klein, O. Ricken, C. Risacher, J. Stutzki, Astrophysical detection of the helium hydride ion  $\text{HeH}^+$ , *Nature* 568 (2019) 357–359.
- [5] D. G. Hopper, The electronic structure of  $\text{HeH}_2^+$ , *Int. J. Quant. Chem. Quant. Chem. Symp.* 12 (1978) 305–322.
- [6] D. Koner, J. C. S. V. Veliz, A. van der Avoird, M. Meuwly, Near dissociation states for  $\text{H}_2^+-\text{He}$  on MRCI and FCI potential energy surfaces, *Phys. Chem. Chem. Phys.* 21 (2019) 24976–24983.
- [7] X. N. Tang, H. Xu, T. Zhang, Y. Hou, C. Chang, C. Y. Ng, Y. Chiu, R. A. Dressler, D. J. Levandier, A pulsed-field ionization photoelectron secondary ion coincidence study of the  $\text{H}_2^+$  ( $X, v^+ = 0-15, N^+ = 1$ ) + He proton transfer reaction, *J. Chem. Phys.* 122 (2005) 164301.
- [8] W. A. Chupka, M. E. Russell, Photoionization study of ion–molecule reactions in mixtures of hydrogen and rare gases, *J. Chem. Phys.* 49 (12) (1968) 5426–5437.
- [9] M. Baer, S. Suzuki, K. Tanaka, I. Koyano, H. Nakamura, Z. Herman, D. J. Kouri, He +  $\text{H}_2^+$  ion-molecule reaction: A comparison between experimental and quantum-mechanical results, *Phys. Rev. A* 34 (1986) 1748–1751.
- [10] T. Turner, O. Dutuit, Y. T. Lee, The effects of collision energy and vibrational excitation on  $\text{H}_2^+$ ,  $\text{HD}^+$  + He reactions, *J. Chem. Phys.* 81 (1984) 3475–3481.
- [11] J. E. Pollard, J. A. Syage, L. K. Johnson, R. B. Cohen, Collinear reactive scattering of state-selected  $\text{H}_2^+ + \text{He} \rightarrow \text{HeH}^+ + \text{H}$ : A method for probing dynamical resonances, *J. Chem. Phys.* 94 (1991) 8615–8617.
- [12] A. Carrington, D. I. Gammie, A. M. Shaw, S. M. Taylor, J. M. Hutson, Observation of a microwave spectrum of the long-range He ...  $\text{H}_2^+$  complex, *Chem. Phys. Lett.* 260 (1996) 395–405.
- [13] D. I. Gammie, J. C. Page, A. M. Shaw, Microwave and millimeter-wave spectrum of the He... $\text{H}_2^+$  long-range complex, *J. Chem. Phys.* 116 (2002) 6072–6078.
- [14] J. Tennyson, S. Miller, Predicted vibration–rotation levels of  $\text{H}_2\text{He}^+$  and its isotopomers, *J. Chem. Phys.* 87 (1987) 6648–6652.
- [15] V. Špirko, W. P. Kraemer, Ab initio predicted rotation–vibration energy levels of  $\text{HeH}_2^+$ , *J. Mol. Spectrosc.* 172 (1995) 265–274.
- [16] M. Jurek, V. Špirko, W. P. Kraemer, Ab initio calculated rotation–vibration line strengths for  $\text{HeH}_2^+$ , *J. Mol. Spectrosc.* 182 (1997) 364–370.
- [17] F. Mrugała, V. Špirko, W. P. Kraemer, Radiative association of  $\text{HeH}_2^+$ , *J. Chem. Phys.* 118 (2003) 10547–10560.
- [18] M. Meuwly, J. M. Hutson, The potential energy surface and near-dissociation states of  $\text{He-H}_2^+$ , *J. Chem. Phys.* 110 (1999) 3418–3427.
- [19] M. Meuwly, J. M. Hutson, Predictions of microwave and far-infrared transitions in  $\text{He-H}_2^+$ , *Mon. Not. Royal Astron. Soc.* 302 (4) (1999) 790–792.
- [20] C. N. Ramachandran, D. De Fazio, S. Cavalli, F. Tarantelli, V. Aquilanti, Revisiting the potential energy surface for the  $\text{He} + \text{H}_2^+ \rightarrow \text{HeH}^+ + \text{H}$  reaction at the full configuration interaction level, *Chem. Phys. Lett.* 469 (2009) 26–30.
- [21] D. De Fazio, M. de Castro-Vitores, A. Aguado, V. Aquilanti, S. Cavalli, The  $\text{He} + \text{H}_2^+ \rightarrow \text{HeH}^+ + \text{H}$  reaction: Ab initio studies of the potential energy surface, benchmark time-independent quantum dynamics in an extended energy range and comparison with experiments, *J. Chem. Phys.* 137 (2012) 244306.
- [22] T. Szidarovszky, K. Yamanouchi, Photodissociation dynamics of weakly bound  $\text{heh}_2^+$  in intense light fields, *Phys. Rev. A* 94 (2016) 6.
- [23] T. Szidarovszky, K. Yamanouchi, Full-dimensional simulation of the laser-induced alignment dynamics of  $\text{H}_2\text{He}^+$ , *Mol. Phys.* 115 (2017) 1916–1926.
- [24] D. Papp, T. Szidarovszky, A. G. Császár, A general variational approach for computing rovibrational resonances of polyatomic molecules. Application to the weakly bound  $\text{H}_2\text{He}^+$  and  $\text{H}_2\text{-CO}$  systems, *J. Chem. Phys.* 147 (2017) 094106.
- [25] D. Papp, A. G. Császár, K. Yamanouchi, T. Szidarovszky, Rovibrational resonances in  $\text{H}_2\text{He}^+$ , *J. Chem. Theory Comput.* 14 (2018) 1523–1533.
- [26] J. Tennyson, M. A. Kostin, P. Barletta, G. J. Harris, O. L. Polyansky, J. Ramanlal, N. F. Zobov, DVR3D: a program suite for the calculation of rotation–vibration spectra of triatomic molecules, *Comput. Phys. Commun.* 163 (2004) 85–116.
- [27] G. C. Groenenboom, P. E. S. Wormer, A. van der Avoird, E. M. Mas, R. Bukowski, K. Szalewicz, Water pair potential of near spectroscopic accuracy: II. Vibration–rotation–tunneling levels of the water dimer, *J. Chem. Phys.* 113 (2000) 6702–6715.
- [28] A. G. Császár, I. Simkó, T. Szidarovszky, G. C. Groenenboom, T. Karman, A. van der Avoird, Rotational–vibrational resonance states, *Phys. Chem. Chem. Phys.* 22 (2020) 15081–15104.
- [29] D. De Fazio, M. de Castro-Vitores, A. Aguado, V. Aquilanti, S. Cavalli, The  $\text{He} + \text{H}_2^+ \rightarrow \text{HeH}^+ + \text{H}$  reaction: Ab initio studies of the potential energy surface, benchmark time-independent quantum dynamics in an extended energy range and comparison with experiments, *J. Chem. Phys.* 137 (2012) 244306.
- [30] P. Jusko, S. Brünken, O. Asvany, S. Thorwirth, A. Stoffels, L. van der Meer, G. Berden, B. Redlich, J. Oomens, S. Schlemmer, The FELion cryogenic ion trap beam line at the FELIX free-electron laser laboratory: infrared signatures of primary alcohol cations, *Faraday Discuss.* 217 (2019) 172–202.
- [31] D. Oepts, A. F. G. van der Meer, P. W. van Amersfoort, The free-electron-laser user facility FELIX, *Infrared Phys. Technol.* 36 (1995) 297–308.
- [32] H. H. Nielsen, The vibration–rotation energies of molecules, *Rev. Mod. Phys.* 23 (1951) 90–136.
- [33] D. Papoušek, M. Aliev, *Molecular Vibrational–Rotational Spectra*, Elsevier, Amsterdam, 1982.
- [34] W. D. Allen, Y. Yamaguchi, A. G. Császár, D. A. Clabo Jr., R. B. Remington, H. F. Schaefer III, A systematic study of molecular vibrational anharmonicity and vibration–rotation interaction by self-consistent-field higher derivative methods. Linear polyatomic molecules, *Chem. Phys.* 145 (1990) 427–466.
- [35] A. G. Császár, T. Szidarovszky, O. Asvany, S. Schlemmer, Fingerprints of microscopic superfluidity in  $\text{HHe}_n^+$  clusters, *Mol. Phys.* 117 (2019) 1559–1583.
- [36] O. Asvany, S. Schlemmer, T. Szidarovszky, A. G. Császár, Infrared signatures of the  $\text{HHe}_n^+$  and  $\text{DHe}_n^+$  ( $n = 3-6$ ) complexes, *J. Phys. Chem. Lett.* 10 (2019) 5325–5330.
- [37] M. Töpfer, A. Jensen, K. Nagamori, H. Kohguchi, T. Szidarovszky, A. G. Császár, S. Schlemmer, O. Asvany, Spectroscopic signatures of  $\text{HHe}_2^+$  and  $\text{HHe}_3^+$ , *Phys. Chem. Chem. Phys.* 22 (2020) 22885–22888.
- [38] O. Asvany, S. Brünken, L. Kluge, S. Schlemmer, COLTRAP: a 22-pole

- ion trapping machine for spectroscopy at 4 K, *Appl. Phys. B* 114 (2014) 203–211.
- [39] O. Asvany, F. Biela, D. Moratschke, J. Krause, S. Schlemmer, New design of a cryogenic linear RF multipole trap, *Rev. Sci. Instr.* 81 (2010) 076102.
- [40] P. R. Bunker, P. Jensen, *Molecular Symmetry and Spectroscopy*, NRC, Ottawa, 1998.
- [41] J. Brown, J. Hougen, K.-P. Huber, J. Johns, I. Kopp, H. Lefebvre-Brion, A. Merer, D. Ramsay, J. Rostas, R. Zare, The labeling of parity doublet levels in linear molecules, *Journal of Molecular Spectroscopy* 55 (1-3) (1975) 500–503.
- [42] M. Kállay, P. R. Surján, Higher excitations in coupled-cluster theory, *J. Chem. Phys.* 115 (2001) 2945.
- [43] CFOUR, a quantum chemical program package written by J. F. Stanton, J. Gauss, M. E. Harding, P. G. Szalay with contributions from A. A. Auer, R. J. Bartlett, U. Benedikt, C. Berger, D. E. Bernholdt, Y. J. Bomble, L. Cheng, O. Christiansen, M. Heckert, O. Heun, C. Huber, T.-C. Jagau, D. Jonsson, J. Jusélius, K. Klein, W. J. Lauderdale, D. A. Matthews, T. Metzroth, D. P. O’Neill, D. R. Price, E. Prochnow, K. Ruud, F. Schiffmann, W. Schwalbach, S. Stopkowitz, A. Tajti, J. Vázquez, F. Wang, J. D. Watts and the integral packages MOLECULE (J. Almlöf and P. R. Taylor), PROPS (P. R. Taylor), ABACUS (T. Helgaker, H.-J. Aa. Jensen, P. Jørgensen, and J. Olsen), and ECP routines by A. V. Mitin and C. van Wüllen. For the current version, see <http://www.cfour.de>.
- [44] MRCC, a quantum chemical program suite written by M. Kállay, Z. Rolik, J. Csontos, P. Nagy, G. Samu, D. Mester, J. Csóka, B. Szabó, I. Ladjánszki, L. Szegedy, B. Ladóczki, K. Petrov, M. Farkas, P. D. Mezei, and B. Hégyel. For the current version, see [www.mrcc.hu](http://www.mrcc.hu).
- [45] Z. Rolik, L. Szegedy, I. Ladjánszki, B. Ladóczki, M. Kállay, An efficient linear-scaling CCSD(T) method based on local natural orbitals, *J. Chem. Phys.* 139 (2013) 094105.
- [46] M. J. Frisch, G. W. Trucks, H. B. Schlegel, G. E. Scuseria, M. A. Robb, J. R. Cheeseman, G. Scalmani, V. Barone, G. A. Petersson, H. Nakatsuji, X. Li, M. Caricato, A. V. Marenich, J. Bloino, B. G. Janesko, R. Gomperts, B. Mennucci, H. P. Hratchian, J. V. Ortiz, A. F. Izmaylov, J. L. Sonnenberg, D. Williams-Young, F. Ding, F. Lipparini, F. Egidi, J. Goings, B. Peng, A. Petrone, T. Henderson, D. Ranasinghe, V. G. Zakrzewski, J. Gao, N. Rega, G. Zheng, W. Liang, M. Hada, M. Ehara, K. Toyota, R. Fukuda, J. Hasegawa, M. Ishida, T. Nakajima, Y. Honda, O. Kitao, H. Nakai, T. Vreven, K. Throssell, J. A. Montgomery, Jr., J. E. Peralta, F. Ogliaro, M. J. Bearpark, J. J. Heyd, E. N. Brothers, K. N. Kudin, V. N. Staroverov, T. A. Keith, R. Kobayashi, J. Normand, K. Raghavachari, A. P. Rendell, J. C. Burant, S. S. Iyengar, J. Tomasi, M. Cossi, J. M. Millam, M. Klene, C. Adamo, R. Cammi, J. W. Ochterski, R. L. Martin, K. Morokuma, O. Farkas, J. B. Foresman, D. J. Fox, *Gaussian 16 Revision B.01*, gaussian Inc. Wallingford CT (2016).
- [47] T. H. Dunning Jr., Gaussian basis sets for use in correlated molecular calculations. I. The atoms boron through neon and hydrogen, *J. Chem. Phys.* 90 (1989) 1007–1023.
- [48] T. Szidarovszky, A. G. Császár, G. Czakó, On the efficiency of treating singularities in triatomic variational vibrational computations. The vibrational states of  $H_3^+$  up to dissociation, *Phys. Chem. Chem. Phys.* 12 (2010) 8373–8386.
- [49] J. C. Light, T. Carrington, Discrete-variable representations and their utilization, *Adv. Chem. Phys.* 114 (2000) 263–310.
- [50] T. Szidarovszky, A. G. Császár, Low-lying quasibound rovibrational states of  $H_2^{16}O$ , *Mol. Phys.* 111 (14-15, SI) (2013) 2131–2146.
- [51] E. R. Davidson, The iterative calculation of a few of the lowest eigenvalues and corresponding eigenvectors of large real-symmetric matrices, *J. Comput. Phys.* 17 (1975) 87–94.
- [52] A. van der Avoird, P. E. S. Wormer, R. Moszynski, From intermolecular potentials to the spectra of Van der Waals molecules, and vice versa, *Chem. Rev.* 94 (1994) 1931–1974.
- [53] A. van der Avoird, D. J. Nesbitt, Rovibrational states of the  $H_2O-H_2$  complex; an *ab initio* calculation, *J. Chem. Phys.* 134 (2011) 044314.
- [54] O. Asvany, S. Schlemmer, Numerical simulations of kinetic ion temperature in a cryogenic linear multipole trap, *Int. J. Mass Spectrom.* 279 (2009) 147–155.
- [55] S. Gärtner, J. Krieg, A. Klemann, O. Asvany, S. Brünken, S. Schlemmer, High-resolution spectroscopy of  $CH_2D^+$  in a cold 22-pole ion trap, *J. Phys. Chem. A* 117 (39) (2013) 9975–9984.
- [56] M. Töpfer, T. Salomon, S. Schlemmer, O. Dopfer, H. Kohguchi, K. M. T. Yamada, O. Asvany, Double resonance rotational spectroscopy of weakly bound ionic complexes: the case of floppy  $CH_3^+-He$ , *Phys. Rev. Lett.* 121 (2018) 143001.
- [57] T. Salomon, M. Töpfer, P. Schreier, S. Schlemmer, H. Kohguchi, L. Surin, O. Asvany, Double resonance rotational spectroscopy of  $He-HCO^+$ , *Phys. Chem. Chem. Phys.* 21 (2019) 3440–3445.
- [58] S. Brünken, L. Kluge, A. Stoffels, O. Asvany, S. Schlemmer, Laboratory rotational spectrum of  $1-C_3H^+$  and confirmation of its astronomical detection, *Astrophys. J. Lett.* 783 (2014) L4.
- [59] J. L. Doménech, S. Schlemmer, O. Asvany, Accurate frequency determination of vibration–rotation and rotational transitions of  $SiH^+$ , *Astrophys. J.* 849 (2017) 60.
- [60] J. L. Doménech, P. Jusko, S. Schlemmer, O. Asvany, The first laboratory detection of vibration-rotation transitions of  $^{12}CH^+$  and  $^{13}CH^+$  and improved measurement of their rotational transition frequencies, *Astrophys. J.* 857 (2018) 61.
- [61] S. Thorwirth, P. Schreier, T. Salomon, S. Schlemmer, O. Asvany, Pure rotational spectrum of  $CN^+$ , *Astrophys. J.* 882 (2019) L6.
- [62] A. Krapp, G. Frenking, E. Uggerud, Nonpolar dihydrogen bonds—On a gliding scale from weak dihydrogen interaction to covalent H–H in symmetric radical cations  $[H_nE-H-H-EH_n]^+$ , *Chem. Eur. J.* 14 (2008) 4028–4038.